



HAL
open science

In vitro identification of imidazo[1,2-a]pyrazine-based antileishmanial agents and evaluation of L. major casein kinase 1 inhibition

Marc-Antoine Bazin, Sandrine Cojean, Fabrice Pagniez, Guillaume Bernadat, Christian Cavé, Isabelle Ourliac-Garnier, Marie-Renée Nourrisson, Cathy Morgado, Carine Picot, Olivier Leclercq, et al.

► To cite this version:

Marc-Antoine Bazin, Sandrine Cojean, Fabrice Pagniez, Guillaume Bernadat, Christian Cavé, et al.. In vitro identification of imidazo[1,2-a]pyrazine-based antileishmanial agents and evaluation of L. major casein kinase 1 inhibition. *European Journal of Medicinal Chemistry*, 2021, 210, pp.112956. 10.1016/j.ejmech.2020.112956 . pasteur-03108849

HAL Id: pasteur-03108849

<https://pasteur.hal.science/pasteur-03108849>

Submitted on 8 Mar 2021

HAL is a multi-disciplinary open access archive for the deposit and dissemination of scientific research documents, whether they are published or not. The documents may come from teaching and research institutions in France or abroad, or from public or private research centers.

L'archive ouverte pluridisciplinaire **HAL**, est destinée au dépôt et à la diffusion de documents scientifiques de niveau recherche, publiés ou non, émanant des établissements d'enseignement et de recherche français ou étrangers, des laboratoires publics ou privés.



Distributed under a Creative Commons Attribution - NonCommercial 4.0 International License

***In vitro* identification of imidazo[1,2-*a*]pyrazine-based antileishmanial agents and evaluation of *L. major* casein kinase 1 inhibition**

Marc-Antoine Bazin ^a, Sandrine Cojean ^b, Fabrice Pagniez ^a, Guillaume Bernadat ^b, Christian Cavé ^b, Isabelle Ourliac-Garnier ^a, Marie-Renée Nourrisson ^a, Cathy Morgado ^a, Carine Picot ^a, Olivier Leclercq ^c, Blandine Baratte ^{d,e}, Thomas Robert ^{d,e}, Gerald F. Späth ^c, Najma Rachidi ^c, Stéphane Bach ^{d,e}, Philippe M. Loiseau ^b, Patrice Le Pape ^a, Pascal Marchand ^{a,*}

^a Université de Nantes, Cibles et médicaments des infections et du cancer, IICiMed, EA 1155, F-44000, Nantes, France

^b BioCIS Biomolécules: Conception, Isolement, Synthèse, Chimiothérapie Antiparasitaire, UMR CNRS 8076, Univ. Paris-Sud, Université Paris-Saclay, Faculté de Pharmacie, F-92296 Châtenay-Malabry, France

^c Institut Pasteur and Institut National de Santé et Recherche Médicale INSERM U1201, Unité de Parasitologie Moléculaire et Signalisation, F-75015 Paris, France

^d Sorbonne Université, CNRS, UMR8227, Integrative Biology of Marine Models Laboratory (LBI2M), Station Biologique de Roscoff, F-29680 Roscoff, France

^e Sorbonne Université, CNRS, FR2424, Kinase Inhibitor Specialized Screening facility - KISSf, Station Biologique, F-29680 Roscoff, France

Keywords: Antileishmanial agents, Casein kinase 1, L-CK1.2 inhibitors, Imidazo[1,2-*a*]pyrazines, Homology model.

*** Corresponding author:**

Université de Nantes, Cibles et Médicaments des Infections et du Cancer, Département de Chimie Thérapeutique, IICiMed, EA 1155, Institut de Recherche de la Santé 2, 22 Boulevard Bénoni Goullin 44200 Nantes, France. E-mail address: pascal.marchand@univ-nantes.fr (P. Marchand)

Abstract:

Leishmaniasis constitutes a severe public health problem, with an estimated prevalence of 12 million cases. This potentially fatal disease has a worldwide distribution and in 2012, the fatal Visceral Leishmaniasis (VL) was declared as new emerging disease in Europe, mainly due to global warming, with expected important public health impact. The available treatments are toxic, costly or lead to parasite resistance, thus there is an urgent need for new drugs with new mechanism of action. Previously, we reported the discovery of **CTN1122**, a potent imidazo[1,2-*a*]pyrazine-based antileishmanial hit compound targeting L-CK1.2 at low micromolar ranges. Here, we described structurally related, safe and selective compounds endowed with antiparasitic properties, better than miltefosine, the reference therapy by oral route. L-CK1.2 homology model gave the first structural explanations of the role of 4-pyridyl (**CTN1122**) and 2-aminopyrimidin-4-yl (compound **21**) moieties, at the position 3 of the central core, in the low micromolar to nanomolar L-CK1.2 inhibition, whereas *N*-methylpyrazole derivative **11** remained inactive against the parasite kinase.

1. Introduction

Leishmaniasis constitutes one of the 20 diseases included in the Neglected Tropical Diseases (NTDs) program of the World Health Organisation (WHO). According to a recent report from WHO [1], the three clinical forms, cutaneous (CL), mucocutaneous (MCL) and visceral leishmaniasis (VL), collectively affect 12 million people in 98 countries, and 1 billion are at risk of infection. Moreover, there are almost 1 million new cases and 30 000 deaths attributed to leishmaniasis each year [2]. Clinical forms differ in immunopathologies, degree of morbidity and mortality. VL is the most severe form of Leishmaniasis, fatal in the absence of treatment, whereas CL is significantly associated with morbidity. Indeed, leishmaniasis-related disabilities impose a great social burden and impair economic productivity; the social stigma associated with the deformities and disfiguring scars often keeps patients hidden. Leishmaniasis has so become a disease, which impedes socio-economic development. CL is more widely distributed than VL, with 70 to 75% of the global estimated CL incidence occurring in ten countries: Afghanistan, Algeria, Brazil, Colombia, Costa Rica, Ethiopia, Iran, Peru, Sudan and Syria. In contrast, more than 90% of VL cases occur in six countries: Bangladesh, Brazil, Ethiopia, India, South Sudan and Sudan [3]. In 2012, VL was declared as new emerging disease in Europe, due mainly to global warming, with an expected important public health impact [4]. According to WHO, despite the measures taken to eradicate leishmaniasis, the number of cases is increasing as well as the mortality. The expansion of leishmaniasis and the alarming rise in number of cases is related to environmental changes such as deforestation, building of dams, new irrigation schemes and migration of non-immune people to endemic areas. The causative agent of Leishmaniasis is a protozoan of the *Leishmania* genus transmitted to its mammalian hosts (humans, dogs, monkeys, rodents...) by the bite of an infected sandfly (*Phlebotominae*). The form of the disease depends upon the species; VL is caused by *Leishmania donovani* and *L. infantum*, CL by species such as *L. major*, *L. amazonensis*, *L. tropica* or *L. mexicana* and MCL by *L. braziliensis* [5]. *Leishmania* parasites present two morphological stages: extracellular flagellated promastigotes in the digestive tract of their sandfly vector and non-motile amastigotes inside the cells of their host mononuclear phagocytic system [2,5].

Despite efforts of the community, there is as yet no effective vaccine in widespread clinical use for prevention of human leishmaniasis [6] and vector control approaches remain extremely difficult [7]. Moreover, only a limited number of drugs are used in the treatment of Leishmaniasis, including pentavalent antimonials, amphotericin B, pentamidine, paromomycin and miltefosine. Miltefosine is the only orally active drug and is highly effective (up to 98% cure rates) [1-3]. Unfortunately, most of these drugs cause side effects, high toxicities and display a high rate of treatment failure in HIV co-infected patients. They are costly, require long-term treatment and lead to parasite resistance [1-3].

In the last decade, efforts have been made by governmental, non-governmental and non-profit organizations to develop leads that moved forward to preclinical and clinical stages of drug discovery, especially against VL, but the drug portfolio is still quite limited [8,9].

In this context, Drug for Neglected Disease initiative (DNDi), through drug repurposing strategy, studied nitroaromatic compounds including nitroimidazole, nitroimidazo-oxazole and nitroimidazo-oxazine derivatives. 7-Substituted nitroimidazo-oxazine compound, identified **DNDI-0690** (Figure 1), displaying very good activity against intramacrophage forms of both *L. donovani* and *L. infantum* ($EC_{50} = 60$ nM and 93 nM, respectively), non-

toxicity (SI > 1000) for mammalian cells and *in vivo* efficacy with high oral bioavailability, entered preclinical trials in September 2015, with the first-in-man studies being carried out by the end 2018 [8,9].

[insert **Figure 1**]

In 2016, the 6-carboxamide benzoxaborole **DNDI-6148** (Figure 1) concluded preclinical VL studies with *in vivo* efficacy compared to miltefosine in mice at a minimum dose of 25 mg/kg/day b.i.d. after a 10-day treatment [8,9]. Nevertheless, its antileishmanial mode of action remains unclear.

DNDi, with support from pharma industry, produced the aminopyrazole urea lead candidate **DNDI-5561** to enter in Phase I clinical trials against VL. Its structure remains unknown but analogues such as **DNDI-1044** and compound **I** (Figure 1) are described in the literature [8,9].

The University of Dundee in collaboration with Glaxo Smith Kline (GSK) developed a novel series of pyrazolopyrimidines. Among them, **GSK-3186899/DDD853651** (Figure 1) showed excellent *in vivo* activity in a mouse model of visceral leishmaniasis with good oral availability and safety profile. In addition, Cdc2-related kinase 12 (CRK12) was identified as druggable target for further optimizations. Its biological data support progression to definitive preclinical studies and further phase I clinical trials [8,9].

Novel concepts towards selection of target and novel drugs are thus urgently needed to overcome the current situation and more efficiently combat and eventually eradicate this deadly disease.

In this context, we identified *Leishmania* casein kinase I paralog 2 (L-CK1.2) as the potential target of 2,3-diarylimidazo[1,2-*a*]azine series [10,11] with antileishmanial activity against *L. major*. Especially, we showed that imidazo[1,2-*a*]pyrazine derivative **CTN1122** (Figure 2) killed intracellular amastigotes at the submicromolar dose and was highlighted as an efficient L-CK1.2 inhibitor (IC₅₀ value of 0.72 μM) with a good selectivity index (SI = 52.5) towards macrophages [11].

[insert **Figure 2**]

Interestingly, L-CK1.2 was validated as a drug target for antileishmanial therapy [12,13]. L-CK1.2 is essential for intracellular parasite survival and is released in macrophages via extracellular vesicles (EVs) [12,14]. Moreover, several evidences suggest that L-CK1.2 has been evolutionary selected to interact with and to phosphorylate host proteins subverting the biological and immune functions of the macrophage [12,15,16]. Thus, targeting L-CK1.2 not only kills the intracellular parasite but because of its role outside of the parasite, could also limit the emergence of parasite resistance.

In previous work, the 4-pyridyl in the C3 position of the imidazo[1,2-*a*]pyrazine central core was proved to be the best substitution to retain CK1 inhibition compared to substituted phenyl rings [11]. Starting from the structure of **CTN1122**, the introduction of other aza(hetero)aryl appendages was considered to study their influence on antileishmanial properties and kinase inhibitory activity (Figure 2). The biological activity of advanced precursors was also evaluated for obtaining further structure activity relationship (SAR) data. Additional information of ligand-protein interactions was provided through homology model of *Lm*CK1. We also compared inhibitory activity of L-CK1.2 *versus* mammalian CK1 in order to foresee potential toxicity due to lack of selectivity (*Lm* vs *Hs*). In parallel, *in vitro* cytotoxicity was measured towards two cell lines (human fibroblast MRC-5 and murine

macrophage RAW264.7). In complement to the study, the determination of *in vivo* toxicity using *Galleria mellonella* larvae guided the choice of the most promising antiparasitic compounds [17].

2. Results and discussion

2.1. Chemistry

The design of the first series of imidazo[1,2-*a*]pyrazines **7-11** (Scheme 1) is considered as the extension of the synthetic work previously described by our group [11].

[insert **Scheme 1**]

Thus, derivatives of the reference compound **CTN1122** were prepared by modifying the nature of the ring at the position 3 of the imidazopyrazine scaffold. Our initial SAR efforts were directed toward the introduction of diverse azaheterocyclic cores to compare with 4-pyridyl ring present on **CTN1122**. Briefly, the obtention of the dihalo key intermediate **5** allowed the sequential functionalization at C-8 by nucleophilic substitution and at C-3 by Suzuki coupling. In the last step, different azaheterocyclic moieties such as 3-pyridine, 5-pyrimidine, 5-(2-aminopyrimidine), 5-indazole or 4-(1-methylpyrazole) were introduced to provide five final compounds **7-11** in low to good yields (Table 1). Poor yields were associated with problems of purification mainly due to the polarity of compounds **7** and **9**.

[insert **Table 1**]

Next, we hypothesized that the introduction of a 2-aminopyrimidin-4-yl moiety, in position 3 of the imidazo[1,2-*a*]pyrazine central core, could lead to significant L-CK1.2 inhibition and parasite cell death [18]. The introduction of such substituent was not possible directly from iodo precursor **6** (Scheme 1) since the corresponding boronic acid was not easily available. As depicted in schemes 2 and 3, the functionalization at the level of the 8-chloro analogs **3** and **4** by direct arylation procedure was interesting since it allowed obtaining various advanced derivatives for broader SAR study both at the C8 and C3 positions of the imidazopyrazine.

[insert **Scheme 2**]

[insert **Scheme 3**]

The synthesis began with the preparation of the 4-iodo-2-(methylsulfonyl)pyrimidine **13** following the procedure described by Majeed and coworkers [19]. Once this iodo derivative in hand we could perform a regioselective direct arylation using Fagnou's conditions [20,21] with compounds **3** and **4** as starting materials. Subsequent amination reaction was carried out with dimethylamine and allowed chlorine displacement at the position 8 and isolation of compounds **16** and **17**. Oxidation of the sulfide group with Oxone® afforded sulfones **18** and **19** which were treated with ammonium hydroxide to give 2-aminopyrimidine derivatives **20** and **21** in moderate yields (scheme 2) [22].

We further incorporated an amino group (NH₂) in the position 8 to verify the influence of the substitution at the level of the nitrogen on the binding mode of the molecule. Indeed, we assume that donor-acceptor sequence

between NH₂/N-7 would behave differently than the *N*-dimethyl substitution in the binding site of the target protein. Compound **15** underwent an amination with ammonia under microwave irradiation to furnish **22** in a quantitative yield. The same oxidation / amination sequence as previously used led to the desired compound **24** (Scheme 3).

2.2. Biological evaluation

2.2.1. *In vitro* antileishmanial activity against intracellular amastigotes

The biological evaluation of compounds **7–11**, **14–17**, **20–22** and **24** was conducted against five different species of *Leishmania* parasite, namely *L. major* and *L. amazonensis* for CL, *L. braziliensis* for MCL (Table 2), *L. infantum* and *L. donovani* for fatal VL (Table 3) in the intramacrophage form. Miltefosine was used as reference drug. The intracellular amastigote model is one of the most important assay for the *in vitro* antileishmanial evaluation, because the amastigote stage is found in mammalian host and its infection causes the clinical manifestations of leishmaniasis [2].

To identify new bioactive compounds against *Leishmania*, **CTN1122** was used as a hit with IC₅₀ values of 0.8 μM and 2.74 μM against *L. major* and *L. donovani* strains, respectively [11]. Low toxicity against macrophages (CC₅₀=42.03 μM) and human MRC-5 cells (CC₅₀>100 μM) was also highlighted. Nevertheless, **CTN1122** showed a modest or poor anti-amastigote response against the three other strains. Notably, differences in the *in vitro* drug sensitivities among *Leishmania* species are a well-known fact that has been reported for current antileishmanial drugs [23].

To investigate the SAR for this potential new chemical class of antiparasitic drugs, the 4-pyridyl part at the C3 position of the imidazo[1,2-*a*]pyrazine ring was selected for modification (compounds **7–11**, **17** and **21**). In addition, the synthetic scheme for the obtention of compound **21** allowed us to produce the intermediate **15** which gave access to compounds **22** and **24**, all the molecules varying from **CTN1122** by the C3 and C8 positions (Scheme 2). We were also interested in verifying the influence of the fluorine present on the 2-phenyl ring (R=F, Scheme 2) towards antiparasitic activity by synthesizing the unsubstituted counterparts (R=H for compounds **14**, **16** and **20**, Scheme 2).

[insert **Table 2**]

[insert **Table 3**]

In a general trend for compounds **7–11**, the replacement of 4-pyridyl ring in **CTN1122** by other azaheterocycle (3-pyridyl, 5-pyrimidinyl, 2-aminopyrimidin-5-yl, 5-indazolyl, 1-methylpyrazol-4-yl) furnished poor active compounds on *L. major*, except *N*-methylpyrazole derivative **11** displaying an IC₅₀ value of 8.99 μM. In the pyrimidin-4-yl sub-series, all the compounds **14–17**, **20**, **22** and **24** remained inactive. Interestingly, only compound **21** that showed improved potency (IC₅₀=8.24 μM) was considered as a close analogue of **CTN1122** by exchanging the 4-pyridyl ring with the 2-aminopyrimidin-4-yl appendage. Its analogue **20** (IC₅₀=28.32 μM), without fluorine atom (R=H), was 3.4 fold less active.

Considering *L. amazonensis*, compound **21** ($IC_{50}=6.12\ \mu\text{M}$) was 4.6 fold more potent than the original hit **CTN1122** ($IC_{50}=28.36\ \mu\text{M}$) and was at the level of the control drug miltefosine ($IC_{50}=4.22\ \mu\text{M}$) (Table 2). All the other tested compounds were proved to be inactive, except the 2-(methylthio)pyrimidin-4-yl derivative **14** ($IC_{50}=3.20\ \mu\text{M}$, $R_8=\text{Cl}$), more potent than the reference, and **16** ($IC_{50}=5.99\ \mu\text{M}$, $R_8=\text{N}(\text{CH}_3)_2$). It should be noted that the results on *L. amazonensis* encompass a reverse structure–activity relationship with respect to the presence of fluorine atom in the pyrimidin-4-yl sub-series. Indeed, when compared to compound **20** ($IC_{50}=28.35\ \mu\text{M}$), its fluoro analogue **21** showed a 3.8 fold increased antileishmanial activity, as previously denoted for *L. major* results. Nevertheless, the introduction of a fluorine atom on compounds **14** and **16** was deleterious for the activity when observing the potency of their respective analogues **15** ($IC_{50}>100\ \mu\text{M}$), unactive and **17** ($IC_{50}=12.49\ \mu\text{M}$), twice less active.

No activity was observed against *L. braziliensis* amastigotes for all the compounds. This strain was also not very sensitive to the reference compound Miltefosine ($IC_{50}=8.33\ \mu\text{M}$) (Table 2).

Table 3 depicted the results obtained against visceral leishmaniasis by using classical *L. infantum* and *L. donovani* strains for the assays. Briefly, before discussing more in depth the antileishmanial activities, it is encouraging to see that four IC_{50} values ranged from 1.27 to 2.74 μM , including **CTN1122** and similar to the reference drug Miltefosine on both VL strains. In addition, two compounds displayed IC_{50} s around 6 μM against *L. infantum*. Indeed, VL is the deadly form of Leishmaniasis, if untreated, and it needs consequently to require particular attention when designing new antileishmanial agents.

Among the seven C3 derivatives of **CTN1122** (compounds **7–11**, **17** and **21**) tested against *L. infantum*, only three compounds showed decreased activity compared to the hit ($IC_{50}=12.80\ \mu\text{M}$), indicating that heteroaromatic modifications on this position could be a promising strategy for enhancing antileishmanial properties. Indeed, introducing 3-pyridyl (**7**), 5-pyrimidinyl (**8**), 2-aminopyrimidin-5-yl (**9**) moieties resulted in unactive compounds ($IC_{50}>50\ \mu\text{M}$) but other modulations were in favour of antiparasitic properties. Indazole derivative **10** displayed the same potency as **CTN1122** whereas its *N*-methylpyrazole counterpart **11** exhibited high potency with an IC_{50} value of 2.60 μM , slightly lower than the reference drug miltefosine. In addition, 2-(methylthio) and 2-aminopyrimidin-4-yl derivatives **17** and **21**, respectively, showed IC_{50} s around 6 μM , twice more active than **CTN1122**. Imidazopyrazine **14**, bearing a chlorine atom at the position C8 and a 2-(methylthio)pyrimidine at the position C3, was highlighted as the most potent compound against *L. infantum* ($IC_{50}=1.93\ \mu\text{M}$), 1.5 fold more active than the reference drug. Again, the incidence of the fluorine atom in *para* position of the C3 phenyl ring remained unclear since it was detrimental when introduced on compound **14** ($IC_{50}>100\ \mu\text{M}$ for compound **15**) and favourable for compounds **16** ($IC_{50}=12.54\ \mu\text{M}$ versus **17**) and **20** ($IC_{50}>100\ \mu\text{M}$ versus **21**).

Regarding *L. donovani* strain, the profile of antiparasitic activity of the tested compounds was almost the same as encountered for *L. infantum* strain but with decreased level of potency for compounds **14**, **16**, **17** and **21** with IC_{50} values ranging from 9.82 to 17.57 μM . It must be denoted that the most active compound **14** against *L. infantum* was 5 fold less active against *L. donovani*. Interestingly, *N*-methylpyrazole derivative **11** remained very active with an IC_{50} value of 1.27 μM , 1.4 times more potent than Miltefosine. Whereas displaying poor activity against *L. infantum* strain, **CTN1122** exhibited a promising IC_{50} value of 2.74 μM .

2.2.2. Cytotoxicity and selectivity index

In order to validate the biological interest of the described series as a source of antileishmanial agents, low cytotoxicity profile is mandatory towards the host cells. In this context, all the compounds were tested on RAW 264.7 macrophages and MRC-5 human fibroblast cells. Tables 2 and 3 show the selectivity index (SI), calculated as the ratio of cytotoxicity (CC₅₀ RAW or CC₅₀ MRC-5) to activity (IC₅₀ value on intracellular amastigotes), and SI>10 is usually required for the candidate to progress to the *in vivo* evaluation [24].

Unfortunately, 8-amino-imidazo[1,2-*a*]pyrazines **22** and **24** showed high cytotoxicity for macrophages with IC₅₀ values of 11.51 and 4.69 μM, respectively. Consequently, such toxicity did not allow measuring intramacrophage antileishmanial activity for compound **24** and must induce some concerns with the interpretation of the biological results for compound **22**. The indazolyl moiety on compound **10** also brought important cytotoxicity on macrophages. Except the three compounds discussed before, no general cytotoxicity was observed on MRC5 cells for all the series and the toxicity on macrophages ranged from 15.95 to 50.64 μM.

We previously denoted the interest of *N*-methylpyrazole derivative **11** as antileishmanial agent active against VL at low micromolar range. Even if its cytotoxicity on macrophages has a significant impact (IC₅₀=15.95 μM), the SI reached 6.1 and 12.6 towards *L. infantum* and *L. donovani*, respectively. In addition, no toxicity was measured on MRC-5 cells. The second promising compound to consider is the 2-aminopyrimidine derivative **21**, structurally close to **CTN1122**. This compound showed phenotypic activity on almost all the strains and was accompanied with a SI from 4.2 to 6.9. 2-(Methylthio)pyrimidine derivative **14** showed a good antiparasitic activity together with an appealing SI *versus* macrophages (SI=15.8 for *L. amazonensis* and SI=26.2 for *L. infantum*).

The greater wax moth, *G. mellonella*, is an insect in the order Lepidoptera which larvae have been widely used for acute toxicity testing as a great alternative to testing in rodents [25]. The results obtained with this alternative model are considered to be comparable to those obtained using mammalian models due to *G. mellonella*'s immune system that is functionally and structurally similar to the mammalian innate immune system [26].

All compounds were tested for their toxicity in *G. mellonella* larvae (Figure 3). Groups of 10 larvae were injected with 10 μL of compound at a dose varying from 10 mg/kg to 50 mg/kg. No compounds were tested at a higher dose due to poor solubility of the compounds and limitation of DMSO percentage in the solvent (<40%). The mortality was recorded daily for 7 days. No reduction of viability (or non significative reduction) and no sign of cuticular darkening were observed for any compounds at a dose of 50 mg/kg. These results indicated no toxic effect.

[insert **Figure 3**]

2.2.3. Kinase inhibitory activity

We identified L-CK1.2 as potential target of the reference compound **CTN1122**, displaying inhibitory potency of 0.72 μM against this parasitic kinase [11]. Thus, as part of our continuous efforts to investigate the mechanism of action responsible of antileishmanial properties and to discover new ligands targeting L-CK1.2, all the compounds were tested for *L. major* CK1 inhibition [10–13]. Besides IC₅₀ values against *LmCK1*, the results presented in Table 4 showed the selectivity profile of the compounds *versus* a human CK1 and, an array of 10 representative human and mammalian protein kinases. Interestingly, the activity on these "off-targets" could allow foreseeing toxicity of the described series in the frame of the therapeutic approach relying on host-pathogen interaction.

[insert **Table 4**]

2.2.3.1. Comparative results between phenotypic screening and CK1 inhibition assays of the antileishmanial imidazo[1,2-a]pyrazines

For compounds **7–9**, the results clearly indicated that the replacement of 4-pyridyl ring in **CTN1122** by 3-pyridyl, 5-pyrimidinyl and 2-aminopyrimidin-5-yl moieties dramatically reduced the effectiveness of **CTN1122** for both antileishmanial and anti-CK1 activities. The promising 1-methylpyrazol-4-yl derivative **11**, as antiparasitic agent against VL (intracellular assays on *L. infantum*: IC₅₀=2.60 μM and *L. donovani*: IC₅₀=1.27 μM), displayed poor activity against *LmCK1* (IC₅₀=12.42 μM), suggesting that its potency is not mediated through CK1 inhibition. In that sub-series, the introduction of a 5-indazolyl azaheterocycle in compound **10** allowed retaining micromolar *LmCK1* inhibition, but 2.6 fold less potent than the reference with deleterious impact on antileishmanial potency. In the pyrimidin-4-yl sub-series, compound **14** behaved nearly as compound **11** since, despite micromolar antileishmanial activity against *L. infantum* and *L. amazonensis*, it showed a moderate IC₅₀ value of 5.00 μM on the targeted protein CK1. Moreover, when comparing 2-(methylthio)pyrimidine derivatives **16**, **17** and **22** with their respective 2-aminopyrimidine counterparts **20**, **21** and **24**, it appears clearly that the amino substitution enhances the CK1 inhibitory potency (100, 24 and 16 times, respectively).

As expected, the introduction of a fluorine atom on the C2 phenyl ring of imidazopyrazine scaffold did not interfere with kinase inhibition since compounds **16 versus 17** and **20 versus 21** showed close potency. Considering the slight difference in the structure, the only result that remains unexplained is the broad antileishmanial activity of compound **21** (IC₅₀s < 10 μM against four strains over five) in comparison to the unactivity of compound **20**. As pharmacokinetic hypothesis, the improved lipophilicity (cLog P (**20**)=2.39 vs cLog P (**21**)=2.53 [27]), due to the presence of the additional fluorine atom, could favour the passive diffusion through the cell membranes to reach the parasite. Finally, 8-amino-imidazo[1,2-a]pyrazines **22** and **24** displayed sub-micromolar and nanomolar activities against *LmCK1* but, as previously denoted, were too toxic for further consideration. Their levels of inhibitory activity were in the same range as the corresponding 8-(*N,N*-dimethylamino)imidazo[1,2-a]pyrazines **17** and **21**, respectively.

2.2.3.2. Selectivity profile over a panel of 11 human and mammalian protein kinases including *HsCK1*

In order to check in early stage kinase selectivity issue, since **CTN1122** displayed IC₅₀ of 0.92 μM against *HsCK1ε* of the host (SI= 1.3 over *LmCK1*, Table 4), and to foreseen potential toxicity, all the compounds were tested against a panel of 11 human and mammalian representative protein kinases including *HsCK1*.

Among the active or very potent compounds **10**, **16**, **20**, **17**, **21**, **22** and **24**, against *LmCK1*, all the analogues showed emerging or high selectivity over *HsCK1*, at the exception of compounds **10** and **22** furnishing poor selectivity. The SI ranged from 3 to 30, for the best compound **20** considering this criterion. It must be denoted that, in the contrary to antiparasitic activity, the presence of an additional fluorine atom in compound **21** decreased the selectivity from 30 to 3.8.

The screening assays over the panel of 10 supplementary kinases highlighted a good selectivity of all the compounds except compounds **22** and **24** displaying micromolar or submicromolar activities against CDK2, CDK5, CDK9, GSK3 and CLK1. Interestingly, compounds **16**, **20** and **21** were also very active on CLK1.

Thus, we assumed that the poor selectivity of compounds **22** and **24** could explain their enhanced cytotoxicity.

2.2.3.3. *In silico* binding study

In order to interpret SAR in the framework of the enzyme inhibition assay, we devised a homology model of *Lm*CK1 based on a crystal structure of *Oryza sativa* CK1 (sharing 75% of sequence identity with *Lm*CK1 ignoring the C-terminal flexible loop, see Figure S1 in Supplementary data). This model building phase was followed by a short molecular dynamics simulation in order to refine the overall structure of the model, as well as to explore ATP binding site conformational space (under the hypothesis that active compounds are competitive inhibitors), so as to take protein flexibility into account during the subsequent docking phase. Ligands were then docked against a representative subset of binding site conformations obtained by active site residues RMSD-based clustering. Combinations exhibiting the best score were retained for further analysis (see Figure S2 in Supplementary data).

Examination of the CK1 binding site showed that a significant part is quite hydrophobic due to the presence of several Leu and Ile residues (Figure 4).

[insert **Figure 4**]

Analysis of the structure calculated for one of the best-ranked complex with **CTN1122** suggests that the 4-pyridyl moiety could penetrate the binding site first and occupy one of the most buried parts of the cavity, where the lone pair beared by the nitrogen atom would interact with a strongly polarized N–H group belonging to the side chain of the Lys40 residue (which is also involved in a salt bridge with Glu54). This hypothesis could explain why altering nitrogen atom location and thus the corresponding lone pair orientation would weaken this interaction for compounds **7**, **8**, **9**, **11**, as a consequence of dramatic decrease of CK1 inhibition. Moreover, the fluorinated aromatic phenyl ring would be accomodated by the above-mentioned lipophilic region of the binding site.

Ligand-bound state molecular dynamics calculations are currently in progress to further assess the stability and likelihood of this binding mode. Similar modelling studies on the structure of the human ortholog of CK1 are also being carried out in order to rationalize *in vitro* finding regarding selectivity.

A similar procedure with compounds **17**, **20**, **21**, **22** and **24** confirmed that substituted pyrimidin-4-yl as R3 groups (Table 4) could still be accomodated by the buried pocket in which they could similarly interact with Lys 40, albeit with a not exactly identical imidazopyrine scaffold position. This is likely due to the slight extra bulk brought by the amino or methylthio substituents. However, the possibility to induce further opening of the pocket in question (which would allow the binding mode of compounds from this subset to accurately match that of **CTN1122**) is expected to be confirmed by the aforementioned in progress ligand bound-state molecular dynamics simulations.

3. Conclusion

Optimization of the hit compound **CTN1122** led to generate 13 new imidazo[1,2-*a*]pyrazine analogues to investigate SAR in the fields of antileishmanial potency and *Lm*CK1 inhibition, mostly by modifying the substitution at the level of the positions 3 and/or 8 of the scaffold. Among the tested compounds on the three clinical forms of leishmaniasis, four of them (compounds **11**, **14**, **17** and **21**) demonstrated promising efficacy on VL with micromolar activity against intracellular *L. infantum* and *L. donovani* strains, better than the reference.

Considering CL, the modulations decreased drastically the potency against *L. major* strain but furnished significantly more active compounds (**14**, **16** and **21**) against *L. amazonensis* strain. Interestingly, all the compounds were characterized by very good safety profile displaying low cytotoxicity *in vitro*, except 8-aminoimidazo[1,2-*a*]pyrazine derivatives **22** and **24**, and *in vivo* on *Galleria mellonella* model. As regards parasitic target, the results of *LmCK1* inhibition assays coupled with binding mode study, through molecular homology model, gave the structural requirement to retain kinase inhibition: whether for the pyridine or pyrimidine ring at the position 3 of the central core, the presence of a nitrogen atom at the position 4' is essential to establish polar interaction with Lys 40 of the protein ATP-binding site. Interestingly, two of the most active compounds **20** and **21** on *LmCK1*, at nanomolar range, showed the highest selectivity towards their human ortholog, in favour of further development. Nevertheless, additional study is mandatory to explain the lack of activity of compound **20** on whole parasite. In this context, efforts are also in progress to lead to a detailed understanding of the mechanism of antileishmanial activity of *N*-methylpyrazole derivative **11** since it was highlighted as the most active compound of the series, on both VL strains, without displaying any kinases inhibition. Thus, *LmCK1* proved to be a valuable parasitic target to work on because compound **21**, for instance, inhibiting *LmCK1* with an IC₅₀ value of 42 nM, with emerging selectivity profile *versus* *HsCK1* and other nine kinases, displayed a broad antileishmanial potency against all the tested strains of CL and VL.

In addition, the results of the biological evaluation demonstrated that imidazo[1,2-*a*]pyrazine heterocycle can be considered as suitable central core in the search for new drugs for the therapy of leishmaniasis.

All the structural findings will contribute to establishing structure activity relationships to guide further design of new compounds, which may include new motifs at the positions 3 and/or 8 of the scaffold to promote antiparasitic activity induced through *LmCK1* inhibition and to enhance selectivity indexes.

Finally, assessment of the bioavailability *in vitro* (ADME) is in progress, for the most promising compounds of this study, to go ahead in their potential development.

4. Experimental protocols

4.1. Chemistry

All commercial reagents were used without further purification. All solvents were reagent or HPLC grade. Analytical TLC was performed on silica gel 60 F254 plates. Open column chromatography was performed on silica gel 60 (70–230 mesh ASTM). The flash column chromatography was performed using a Reveleris® X2 Buchi system, with Buchi cartridge (FlashPure 12g, 40 µm irregular silica). Yields refer to chromatographically and spectroscopically pure compounds. Melting points were determined on an Electrothermal melting point apparatus. ¹H NMR and ¹³C NMR spectra were recorded in CDCl₃ or in DMSO-*d*₆ on a 400 MHz spectrometer. Chemical shifts are reported as δ values in parts per million (ppm) relative to tetramethylsilane as internal standard and coupling constants (*J*) are given in hertz. Multiplicities are reported as follows: s = singlet, d = doublet, dd = doublet of doublets, t = triplet, mt = multiplet, bs = broad singlet, t_{app} = apparent triplet. Low resolution mass spectra were recorded using an Electrospray Ionization (ESI) Method with Waters ZQ 2000 spectrometer. UPLC column used was an Acquity UPLC® BEH Phenyl (2.1 mm i.d., 50 mm length, 1.7 µm particle size) from Waters. A linear mobile phase gradient was used with a mobile phase A as 100% of acetonitrile in water (at 2%) and mobile

phase B as 100% acetonitrile. The gradient table was: 0-0.5 min, 0% B; 0.5-4.0 min 0→100% B; 4.0-5.5% 100% B; 5.5-5.7 min 100→0% B; 5.7-7.5 min 0% B. at flow rate 0.5 mL.min⁻¹ and column temperature 35 °C. Formic acid (0.1%) was added in diluent to improve ionization. Pure compounds **7-11** were analyzed at 1 mg/mL in UPLC grade MeOH (Biosolve), following a 5 µL injection on a UFLC-ESIHRMS (IT-TOFMS) Shimadzu instrument (Prominence Ultra Fast Liquid Chromatography coupled to High Resolution Electrospray Ionization Mass Spectrometry combining Ion trap and Time of Flight analyzers). Analyses were performed by Flow Injection (FIA) in the isocratic flow consisting of H₂O/Acetonitrile 85:15 (V/V) at 300 µL/min. The detection using ESI was performed both in positive and negative ionization modes in the mass range m/z 100–1000 with a mass accuracy of 7 ppm and a resolution of 10,000 at m/z 500. For compounds **14-17** and **20-24**, high resolution mass spectrometry (HRMS) was recorded on a Waters Xevo G2-XS Qtof spectrometer (coupled with an HPLC Acquity H-Class) for ESI. Microwave reactions were carried out in a CEM Discover microwave reactor in sealed vessels (monowave, maximum power 300 W, temperature control via IR-sensor, fixed temperature). Compounds **2-6** were synthesized following procedures previously described [9].

4.1.1. General procedure for the synthesis of compounds **7-11**

In a vial were added 2-(4-fluorophenyl)-3-iodo-*N,N*-dimethylimidazo[1,2-*a*]pyrazin-8-amine **6** (1 equiv.), boronic acid (1.1 equiv.), K₃PO₄ (2.5 equiv.) in a 1,4-dioxane/water mixture (9:1, 15 mL). The vial was purged twice with N₂ for 10 minutes, before and after addition of PdCl₂(dppf) (0.05 equiv.). The vial was sealed and the suspension was then heated at 100 °C for 19–23 h. After cooling, the resulting mixture was diluted with EtOAc and water and the organic layer was extracted twice with EtOAc. The combined organic layers were washed with brine, dried over Na₂SO₄, filtered and concentrated under vacuum. The crude product was then purified by chromatography to provide **7-11**.

4.1.1.1. 2-(4-Fluorophenyl)-*N,N*-dimethyl-3-(pyridin-3-yl)imidazo[1,2-*a*]pyrazin-8-amine (**7**)

The reaction was carried out using compound **6** (0.147 g, 0.39 mmol), 3-pyridylboronic acid (0.052 g, 0.42 mmol), K₃PO₄ (0.200 g, 0.96 mmol) and PdCl₂(dppf) (0.020 g, 0.04 mmol) in a 1,4-dioxane/water mixture (9:1, 15 mL) and the reaction was stirred for 22 h. The product was purified by silica gel column chromatography using DCM/EtOH (98:2) as eluent and the compound **7** (34% yield) was obtained as a grey powder. Mp: 139.8 °C; ¹H NMR (400 MHz, CDCl₃) δ 8.75 (d, ³J = 4.0 Hz, 1H), 8.69 (s, 1H), 7.76 (ddd, ³J = 8.0 Hz, ⁴J = 2.0 Hz, ⁴J = 2.0 Hz, 1H), 7.57 (mt, 2H), 7.48 (dd, ³J = 8.0 Hz, ⁴J = 4.0 Hz, 1H), 7.35 (d, ³J = 4.4 Hz, 1H), 7.17 (d, ³J = 4.4 Hz, 1H), 6.99 (mt, 2H), 3.65 (s, 6H); ¹³C NMR (100 MHz, DMSO-*d*₆) δ 161.72 (¹J_{C-F} = 243 Hz), 150.88, 150.26, 149.60, 139.40, 138.38, 133.05, 129.88 (⁴J_{C-F} = 3 Hz), 129.29 (³J_{C-F} = 8 Hz, 2C), 128.78, 125.11, 124.47, 119.15, 115.48 (²J_{C-F} = 22 Hz, 2C), 107.45, 39.35 (2C); MS (ESI) *m/z* (%): 334.2 (100) [M+H]⁺; UPLC purity = 100%, Rt 1.84 min; HRMS (TOF MS ES⁺): calcd. for C₁₉H₁₆FN₅ [M+H]⁺ 334.1463, found: 334.1461.

4.1.1.2. 2-(4-Fluorophenyl)-*N,N*-dimethyl-3-(pyrimidin-5-yl)imidazo [1,2-*a*]pyrazin-8-amine (**8**)

The reaction was carried out using compound **6** (0.350 g, 0.91 mmol), 5-pyrimidylboronic acid (0.125 g, 1.01 mmol), K₃PO₄ (0.486 g, 2.29 mmol) and PdCl₂(dppf) (0.034 g, 0.05 mmol). in a 1,4-dioxane/water mixture (9:1, 15 mL) and the reaction was stirred for 22 h. The product was purified by silica gel column chromatography using DCM/EtOH (99:1) as eluent and the compound **8** (67% yield) was obtained as a beige powder. Mp: 124.4 °C; ¹H NMR (400 MHz, DMSO-*d*₆) 9.36, (s, 1H), 8.97 (s, 2H), 7.55 (mt, 2H), 7.48 (d, ³*J* = 4.4 Hz, 1H), 7.36 (d, ³*J* = 4.4 Hz, 1H), 7.21 (mt, 2H), 3.55 (s, 6H); ¹³C NMR (100 MHz, DMSO-*d*₆) δ 161.80 (¹*J*_{C-F} = 244 Hz), 158.55, 158.46 (2C), 149.54, 140.32, 133.38, 129.32 (⁴*J*_{C-F} = 3 Hz), 129.51 (³*J*_{C-F} = 8 Hz, 2C), 128.88, 123.91, 116.09, 115.58 (²*J*_{C-F} = 21 Hz, 2C), 107.75, 39.80 (2C); MS (ESI) *m/z* (%): 335.1 (100) [M+H]⁺; UPLC purity = 100%, Rt 1.92 min; HRMS (TOF MS ES⁺): calcd. for C₁₈H₁₅FN₆ [M+H]⁺ 335.1415, found: 335.1419.

4.1.1.3. 3-(2-Aminopyrimidin-5-yl)-2-(4-fluorophenyl)-*N,N*-dimethylimidazo[1,2-*a*]pyrazin-8-amine (**9**)

The reaction was carried out using compound **6** (0.300 g, 0.79 mmol), 2-amino-5-pyrimidylboronic acid (0.120 g, 0.86 mmol), K₃PO₄ (0.410 g, 1.96 mmol) and PdCl₂(dppf) (0.030 g, 0.04 mmol). in a 1,4-dioxane/water mixture (9:1, 15 mL) and the reaction was stirred for 22 h. The product was purified by flash column chromatography using cyclohexane/AcOEt (1:1) as eluent and the compound **9** (24% yield) was obtained as a beige powder. Mp: 200.4 °C; ¹H NMR (400 MHz, DMSO-*d*₆) 8.30 (s, 2H), 7.66 (mt, 2H), 7.36 (d, ³*J* = 4.4 Hz, 1H), 7.31 (d, ³*J* = 4.4 Hz, 1H), 7.23 (mt, 2H), 7.14 (s, 2H), 3.53 (s, 6H); ¹³C NMR (100 MHz, DMSO-*d*₆) δ 163.50, 160.04 (¹*J*_{C-F} = 242 Hz), 159.67 (2C), 149.51, 139.32, 132.95, 130.17 (⁴*J*_{C-F} = 3 Hz), 129.06 (³*J*_{C-F} = 8 Hz, 2C), 128.42, 117.65, 115.44 (²*J*_{C-F} = 21 Hz, 2C), 110.98, 107.78, 39.02 (2C); MS (ESI) *m/z* (%): 350.1 (100) [M+H]⁺; UPLC purity = 100%, Rt 1.74 min; HRMS (TOF MS ES⁺): calcd. for C₁₈H₁₆FN₇ [M+H]⁺ 350.1524, found: 350.1520.

4.1.1.4. 2-(4-Fluorophenyl)-3-(1*H*-indazol-5-yl)-*N,N*-dimethylimidazo[1,2-*a*]pyrazin-8-amine (**10**)

The reaction was carried out using compound **6** (0.200 g, 0.52 mmol), 1*H*-indazole-5-boronic acid (0.093 g, 0.58 mmol), K₃PO₄ (0.278 g, 1.36 mmol) and PdCl₂(dppf) (0.019 g, 0.026 mmol). in a 1,4-dioxane/water mixture (9:1, 15 mL) and the reaction was stirred for 23 h. The product was purified by silica gel column chromatography using DCM/EtOH (98:2) as eluent and the compound **10** (77% yield) was obtained as a beige powder. Mp: 131.3 °C; ¹H NMR (400 MHz, DMSO-*d*₆) 13.35 (s, 1H), 8.18 (s, 1H), 7.93 (s, 1H), 7.75 (d, ³*J* = 8.4 Hz, 1H), 7.59 (dd, ³*J* = 8.8 Hz, ³*J* = 5.6 Hz, 2H), 7.35 (dd, ³*J* = 8.4 Hz, ⁴*J* = 1.2 Hz, 1H), 7.28 (d, ³*J* = 4.8 Hz, 1H), 7.23 (d, ³*J* = 4.8 Hz, 1H), 7.13 (mt, 2H), 3.56 (s, 6H); ¹³C NMR (100 MHz, DMSO-*d*₆) δ 161.47 (¹*J*_{C-F} = 243 Hz), 149.55, 139.82, 138.26, 134.12, 132.44, 130.32 (⁴*J*_{C-F} = 3 Hz), 128.89 (³*J*_{C-F} = 8 Hz, 2C), 128.34, 128.12, 123.50, 123.23, 122.70, 120.31, 115.24 (²*J*_{C-F} = 22 Hz, 2C), 111.59, 107.49, 39.06 (2C); MS (ESI) *m/z* (%): 373.1 (100) [M+H]⁺; UPLC purity = 100%, Rt 2.14 min; HRMS (TOF MS ES⁺): calcd. for C₂₁H₁₇FN₆ [M+H]⁺ 371.1426, found: 371.1425.

4.1.1.5. 2-(4-Fluorophenyl)-*N,N*-dimethyl-3-(1-methyl-1*H*-pyrazol-4-yl)imidazo[1,2-*a*]pyrazin-8-amine (**11**)

The reaction was carried out using compound **6** (0.250 g, 0.65 mmol), 1-methyl-1*H*-pyrazole-4-boronic acid (0.150 g, 0.72 mmol), K₃PO₄ (0.347 g, 1.63 mmol) and PdCl₂(dppf) (0.024 g, 0.032 mmol). in a 1,4-dioxane/water mixture (9:1, 15 mL) and the reaction was stirred for 19 h. The product was purified by silica gel column chromatography

using petroleum ether/EtOAc (3:1) as eluent and the compound **11** (85% yield) was obtained as a light beige powder. Mp: 125.0 °C; ¹H NMR (400 MHz, DMSO-*d*₆) 8.07 (s, 1H), 7.73 (mt, 2H), 7.61 (s, 1H), 7.31 (s, 2H), 7.20 (mt, 2H), 3.95 (s, 3H), 3.52 (s, 6H); ¹³C NMR (100 MHz, DMSO-*d*₆) δ 161.60 (¹J_{C-F} = 243 Hz), 149.48, 139.32, 138.94, 132.78, 131.63, 130.43 (⁴J_{C-F} = 3 Hz), 128.98 (³J_{C-F} = 8 Hz, 2C), 128.26, 115.26 (²J_{C-F} = 21 Hz, 2C), 114.65, 107.77, 39.25 (2C), 38.82; MS (ESI) *m/z* (%): 337.1 (100) [M+H]⁺; UPLC purity = 100%, Rt 1.93 min; HRMS (TOF MS ES⁺): calcd. for C₁₈H₁₇FN₆ [M+H]⁺ 373.1571, found: 373.1570.

4.1.2. 4-Iodo-2-(methylsulfanyl)pyrimidine (**13**)

4-Chloro-2-(methylsulfanyl)pyrimidine **12** (10.00 g, 62.3 mmol) was added to HI (57% in water, 50 mL). The reaction mixture was stirred at room temperature for 72 h. After filtration, the precipitate was dissolved in water (50 mL), and the pH mixture was adjusted to 8 with NaHCO₃. The aqueous layer was extracted with CH₂Cl₂ and the organic layer was washed with saturated aqueous solution of Na₂S₂O₃ and water, dried over Na₂SO₄, filtered, and concentrated under reduced pressure. Trituration with petroleum ether afforded **13** (14.85 g, 95% yield) as a white powder. Mp: 51–52 °C (lit. 52–53 °C) [17]; ¹H NMR (400 MHz, CDCl₃) δ 7.99 (d, ³J = 5.1 Hz, 1H, H₆), 7.39 (d, ³J = 5.1 Hz, 1H, H₅), 2.53 (s, 3H, SCH₃).

4.1.3. General procedure for the synthesis of compounds **14–15**

In a vial were added 2-aryl-8-chloroimidazo[1,2-*a*]pyrazine (1 equiv.), compound **13** (2 equiv.), Pd(OAc)₂ (0.2 equiv.), PPh₃ (0.4 equiv.), Cs₂CO₃ (1.5 equiv.) in DMF. The vial was sealed and purged with N₂ through the septum inlet for 10 min. The suspension was then heated at 90 °C for 15–20 h. After cooling, the resulting mixture was diluted with EtOAc and water and the organic layer was extracted twice with EtOAc. The combined organic layers were washed with water, dried over Na₂SO₄, filtered and concentrated under vacuum. The crude product was then purified by flash column chromatography to provide **14–15**.

4.1.3.1. 8-Chloro-3-[2-(methylsulfanyl)pyrimidin-4-yl]-2-phenylimidazo[1,2-*a*]pyrazine (**14**)

The reaction was carried out using 8-chloro-2-phenylimidazo[1,2-*a*]pyrazine **3** (2.00 g, 8.7 mmol), compound **13** (4.39 g, 17.4 mmol), Pd(OAc)₂ (0.39 g, 1.7 mmol), PPh₃ (0.91 g, 3.5 mmol), Cs₂CO₃ (4.26 g, 13.1 mmol) in DMF (20 mL) and the reaction mixture was heated for 20 h. Purification by flash column chromatography using cyclohexane/AcOEt (90:10) as eluent afforded **14** (0.97 g, 31% yield) as a yellow powder. Mp: 178–179 °C; ¹H NMR (400 MHz, CDCl₃) δ 9.39 (d, ³J = 4.8 Hz, 1H), 8.39 (d, ³J = 5.2 Hz, 1H), 7.86 (d, ³J = 4.8 Hz, 1H), 7.67–7.65 (m, 2H), 7.48–7.45 (m, 3H), 6.89 (d, ³J = 5.6 Hz, 1H), 2.66 (s, 3H); ¹³C NMR (100 MHz, CDCl₃) δ 173.10, 157.24, 156.31, 150.68, 143.87, 138.64, 132.98, 129.62, 129.54 (2C), 129.20, 128.97 (2C), 120.44, 119.49, 115.21, 14.23; MS (TOF MS ES⁺) *m/z* (%): 354.06 (100) [M+H]⁺, 376.04 [M+H+Na]⁺; UPLC purity = 98%, Rt 2.89 min; HRMS (TOF MS ES⁺): calcd. for C₁₇H₁₂ClN₅S [M+H]⁺ 354.0580, found: 354.0569.

4.1.3.2. 8-Chloro-2-(4-fluorophenyl)-3-[2-(methylsulfanyl)pyrimidin-4-yl]imidazo[1,2-*a*]pyrazine (**15**)

The reaction was carried out using 8-chloro-2-(4-fluorophenyl)imidazo[1,2-*a*]pyrazine **4** (0.50 g, 2.0 mmol), compound **13** (1.02 g, 4.0 mmol), Pd(OAc)₂ (0.09 g, 0.4 mmol), PPh₃ (0.21 g, 0.8 mmol), Cs₂CO₃ (0.99 g, 3.0 mmol) in DMF (5 mL) and the reaction mixture was heated for 15 h. Purification by flash column chromatography using cyclohexane/AcOEt (1:1) as eluent afforded **15** (0.35 g, 47% yield) as an orange powder. Mp: 188–189 °C; ¹H NMR (400 MHz, CDCl₃) δ 9.36 (d, ³*J* = 4.8 Hz, 1H), 8.43 (d, ³*J* = 5.2 Hz, 1H), 7.88 (d, ³*J* = 4.8 Hz, 1H), 7.68–7.64 (m, 2H), 7.20–7.16 (m, 2H), 6.90 (d, ³*J* = 5.2 Hz, 1H), 2.68 (s, 3H); ¹³C NMR (100 MHz, CDCl₃) δ 173.15, 163.68 (¹*J*_{C-F} = 248 Hz), 156.94, 156.37, 149.70, 143.90, 131.50 (³*J*_{C-F} = 8 Hz, 2C), 129.41, 128.94, 120.35, 119.40, 116.21 (²*J*_{C-F} = 21 Hz, 2C), 115.04, 14.28; MS (TOF MS ES+) *m/z* (%): 372.05 (100) [M+H]⁺; UPLC purity = 99%, Rt 3.08 min; HRMS (TOF MS ES+): calcd. for C₁₇H₁₁ClFN₅S [M+H]⁺ 372.0486, found: 372.0475.

4.1.4. General procedure for the synthesis of compounds **16–17**

In a vial were added compound **14** or **15** (1 equiv.), dimethylamine (40% in water, 20 equiv.), K₂CO₃ (1 equiv.) in DMF. The vial was sealed and the suspension was heated at 90 °C for 4–17 h. After cooling, the resulting mixture was diluted with EtOAc and water and the organic layer was extracted twice with EtOAc. The combined organic layers were washed with water, dried over Na₂SO₄, filtered and concentrated under vacuum. The crude product was then purified by flash column chromatography to provide **16–17**.

4.1.4.1. *N,N*-Dimethyl-3-[2-(methylsulfonyl)pyrimidin-4-yl]-2-phenylimidazo[1,2-*a*]pyrazin-8-amine (**16**)

The reaction was carried out using compound **14** (500 mg, 1.4 mmol), dimethylamine (40% in water, 1.4 mL, 28.2 mmol), K₂CO₃ (195 mg, 1.4 mmol) in DMF (15 mL) and the reaction mixture was heated for 17 h. Purification by flash column chromatography using cyclohexane/AcOEt (90:10) as eluent afforded **16** (282 mg, 55% yield) as a yellow powder. Mp: 136–137 °C; ¹H NMR (400 MHz, CDCl₃) δ 8.57 (d, ³*J* = 4.6 Hz, 1H), 8.33 (d, ³*J* = 5.3 Hz, 1H), 7.64–7.61 (m, 2H), 7.48 (d, ³*J* = 4.7 Hz, 1H), 7.42–7.41 (m, 3H), 6.86 (d, ³*J* = 5.3 Hz, 1H), 3.59 (s, 6H, -N(CH₃)₂), 2.64 (s, 3H); ¹³C NMR (100 MHz, CDCl₃) δ 173.05, 157.33, 157.04, 150.26, 146.63, 134.95, 134.06, 129.37 (2C), 128.97, 128.90 (2C), 119.33, 116.00, 110.11, 77.36, 40.46 (2C), 14.37; MS (TOF MS ES+) *m/z* (%): 363.14 (100) [M+H]⁺; UPLC purity = 98%, Rt 2.50 min; HRMS (TOF MS ES+): calcd. for C₁₉H₁₈N₆S [M+H]⁺ 363.1392, found: 363.1381.

4.1.4.2. 2-(4-Fluorophenyl)-*N,N*-dimethyl-3-[2-(methylsulfonyl)pyrimidin-4-yl]imidazo[1,2-*a*]pyrazin-8-amine (**17**)

The reaction was carried out using compound **15** (220 mg, 0.6 mmol), dimethylamine (40% in water, 0.6 mL, 11.8 mmol), K₂CO₃ (82 mg, 0.6 mmol) in DMF (10 mL) and the reaction mixture was heated for 4 h. Purification by flash column chromatography using cyclohexane/AcOEt (1:1) as eluent afforded **17** (131 mg, 58% yield) as a yellow powder. Mp: 141–142 °C; ¹H NMR (400 MHz, CDCl₃) δ 8.52 (d, ³*J* = 5.2 Hz, 1H), 8.39 (d, ³*J* = 5.2 Hz, 1H), 7.62–7.59 (m, 2H), 7.51 (d, ³*J* = 5.2 Hz, 1H), 7.14–7.11 (m, 2H), 6.86 (d, ³*J* = 5.2 Hz, 1H), 3.68 (s, 6H), 2.63 (s, 3H); ¹³C NMR (100 MHz, CDCl₃) δ 173.17, 163.18 (¹*J*_{C-F} = 247 Hz), 157.06, 156.94, 149.76, 145.43, 134.62, 131.00 (³*J*_{C-F} = 8 Hz, 2C), 129.88, 128.09, 119.31, 115.84 (²*J*_{C-F} = 22 Hz, 2C), 115.73, 109.89, 40.49 (2C), 14.28;

MS (TOF MS ES+) m/z (%): 381.13 (100) [M+H]⁺; UPLC purity = 100%, Rt 2.38 min; HRMS (TOF MS ES+): calcd. for C₁₉H₁₇FN₆S [M+H]⁺ 381.1298, found: 381.1284.

4.1.5. General procedure for the synthesis of compounds **18–19**

In a three-neck round-bottom flask was added compound **16** or **17** (1 equiv.) in methanol. Oxone® dissolved in water was then added dropwise and the suspension was stirred vigorously at room temperature for 17–24h. The resulting mixture was evaporated under reduced pressure. The residue was diluted with EtOAc and the organic layer was washed with a saturated aqueous NaHCO₃ solution, water, dried over Na₂SO₄, filtered and concentrated under vacuum. The crude product was used for the next step without further purification.

4.1.5.1. *N,N*-Dimethyl-3-[2-(methylsulfonyl)pyrimidin-4-yl]-2-phenylimidazo[1,2-*a*]pyrazin-8-amine (**18**)

The reaction was carried out using compound **16** (0.40 g, 1.1 mmol) in MeOH (19 mL), Oxone® (1.02 g, 3.3 mmol) in water (18 mL) and the reaction was stirred for 17 h. The crude product (426 mg, 98% yield) was obtained as a yellow powder. ¹H NMR (400 MHz, CDCl₃) δ 8.87 (d, ³*J* = 4.0 Hz, 1H), 8.62 (d, ³*J* = 4.0 Hz, 1H), 7.64–7.60 (m, 3H), 7.50–7.49 (m, 3H), 7.38 (d, ³*J* = 5.6 Hz, 1H), 7.26 (d, ³*J* = 5.6 Hz, 1H), 3.66 (s, 6H), 3.42 (s, 3H); MS (ESI) m/z (%): 395.1 (100) [M+H]⁺; UPLC purity = 99%, Rt 2.09 min.

4.1.5.2. 2-(4-Fluorophenyl)-*N,N*-dimethyl-3-[2-(methylsulfonyl)pyrimidin-4-yl]imidazo[1,2-*a*]pyrazin-8-amine (**19**)

The reaction was carried out using compound **17** (130 mg, 0.34 mmol) in MeOH (5.9 mL), Oxone® (315 mg, 1.03 mmol) in water (5.5 mL) and the reaction was stirred for 24 h. The crude product (42 mg, 30% yield) was obtained as a yellow powder. ¹H NMR (400 MHz, CDCl₃) δ 8.84 (d, ³*J* = 4.8 Hz, 1H), 8.63 (d, ³*J* = 4.9 Hz, 1H), 7.63–7.59 (m, 3H), 7.36 (d, ³*J* = 4.9 Hz, 1H), 7.18 (t_{app}, ³*J*_{app} = 8.8 Hz, 2H), 3.60 (s, 6H), 3.43 (s, 3H); MS (ESI) m/z (%): 413.1 (100) [M+H]⁺; UPLC purity = 97%, Rt 2.07 min.

4.1.6. General procedure for the synthesis of compounds **20–21**

In a vial were added compound **18** or **19**, ammonium hydroxide (25% in water) in 1,4-dioxane. The vial was sealed and the suspension was heated at 110 °C for 1 h 30–9 h. After cooling, the resulting mixture was diluted with EtOAc and water and the organic layer was washed with water, dried over Na₂SO₄, filtered and concentrated under vacuum. The crude product was then purified by chromatography to provide **20–21**.

4.1.6.1. 3-(2-Aminopyrimidin-4-yl)-*N,N*-dimethyl-2-phenylimidazo[1,2-*a*]pyrazin-8-amine (**20**)

The reaction was carried out using compound **18** (200 mg, 0.51 mmol), ammonium hydroxide (25% in water, 5 mL) in 1,4-dioxane (5 mL) and the reaction mixture was heated for 9 h. Purification by flash column chromatography using cyclohexane/AcOEt (1:1) as eluent afforded **20** (85 mg, 51% yield) as a white powder. Mp:

224–225 °C; ¹H NMR (400 MHz, CDCl₃) δ 8.47 (d, ³J = 4.8 Hz, 1H), 8.17 (d, ³J = 4.9 Hz, 1H), 7.68–7.65 (m, 2H), 7.45 (d, ³J = 4.8 Hz, 1H), 7.42–7.39 (m, 3H), 6.57 (d, ³J = 4.9 Hz, 1H), 5.25 (bs, 2H), 3.60 (s, 6H); ¹³C NMR (100 MHz, CDCl₃) δ 162.87, 158.40, 158.26, 150.53, 145.37, 134.71, 134.19, 129.20 (2C), 128.90, 128.53 (2C), 128.46, 119.32, 111.92, 109.82, 39.98 (2C); MS (TOF MS ES+) m/z (%): 332.16 (100) [M+H]⁺; UPLC purity = 98%, Rt 1.77 min; HRMS (TOF MS ES+): calcd. for C₁₈H₁₇N₇ [M+H]⁺ 332.1624, found: 332.1614.

4.1.6.2. 3-(2-Aminopyrimidin-4-yl)-2-(4-fluorophenyl)-N,N-dimethylimidazo[1,2-a]pyrazin-8-amine (**21**)

The reaction was carried out using compound **19** (84 mg, 0.20 mmol), ammonium hydroxide (25% in water, 3 mL) in 1,4-dioxane (3 mL) and the reaction mixture was heated for 1 h 30. Purification by flash chromatography (dichloromethane/ethanol, 98:2) afforded **21** (52 mg, 73% yield) as a white powder. Mp: 172–173 °C; ¹H NMR (400 MHz, CDCl₃) δ 8.44 (d, ³J = 4.8 Hz, 1H), 8.20 (d, ³J = 5.6 Hz, 1H), 7.66–7.63 (m, 2H), 7.46 (d, ³J = 4.4 Hz, 1H), 7.12–7.08 (m, 2H), 6.56 (d, ³J = 5.2 Hz, 1H), 5.24 (bs, 2H), 3.60 (s, 6H); ¹³C NMR (100 MHz, CDCl₃) δ 163.00 (¹J_{C-F} = 247 Hz), 162.90, 158.40, 158.24, 150.41, 144.31, 134.62, 130.94 (³J_{C-F} = 8 Hz, 2C), 130.22, 128.89, 119.28, 115.59 (²J_{C-F} = 22 Hz, 2C), 111.77, 109.74, 40.02 (2C); MS (TOF MS ES+) m/z (%): 350.15 (100) [M+H]⁺; UPLC purity = 100%, Rt 1.83 min; HRMS (TOF MS ES+): calcd. for C₁₉H₁₈N₆S [M+H]⁺ 350.1529, found: 350.1517.

4.1.7. 2-(4-Fluorophenyl)-3-[2-(methylsulfonyl)pyrimidin-4-yl]imidazo[1,2-a]pyrazin-8-amine (**22**)

In a vial were added compound **15** (0.125 g, 0.34 mmol), ammonium hydroxide (3.3 mL, 25% in water) and isopropanol (1.6 mL). The vial was sealed and heated under microwave irradiation at 120 °C for 1 h (P = 80 W). After cooling, water was added and the resulting precipitate was filtered off. The filtrate was extracted with dichloromethane and the organic layer was dried over Na₂SO₄, filtered and concentrated under vacuum. The combined solids were washed with diisopropyl ether to provide **22** (0.118 g, 100% yield) as a beige powder. Mp: 185–186 °C; ¹H NMR (400 MHz, CDCl₃) δ 8.70 (d, ³J = 5.0 Hz, 1H), 8.37 (d, ³J = 5.0 Hz, 1H), 7.61 (dd, ³J = 8.4 Hz, ³J = 5.2 Hz, 2H), 7.47 (d, ³J = 4.8 Hz, 1H), 7.16 (mt, 2H), 6.83 (d, ³J = 5.2 Hz, 1H), 5.72 (s, 2H), 2.65 (s, 3H); ¹³C NMR (100 MHz, CDCl₃) δ 173.10, 163.32 (¹J_{C-F} = 248 Hz), 157.00, 156.80, 149.78, 146.93, 133.37, 131.11 (³J_{C-F} = 8 Hz, 2C), 129.84 (⁴J_{C-F} = 4 Hz), 129.43, 120.08, 116.07 (²J_{C-F} = 22 Hz, 2C), 114.98, 111.92, 14.21; MS (TOF MS ES+) m/z (%): 353.10 (100) [M+H]⁺; UPLC purity = 97%, Rt 2.09 min; HRMS (TOF MS ES+): calcd. for C₁₇H₁₃FN₆S [M+H]⁺ 353.0985, found: 353.0979.

4.1.8. 2-(4-Fluorophenyl)-3-[2-(methylsulfonyl)pyrimidin-4-yl]imidazo[1,2-a]pyrazin-8-amine (**23**)

In a round-bottom flask was dissolved compound **22** (100 mg, 0.34 mmol) in MeOH (4.6 mL). Oxone® (263 mg, 0.85 mmol) in water (4.6 mL) was added and the reaction was stirred at room temperature for 24 h. The resulting mixture was evaporated under reduced pressure. Water was added and the mixture was extracted with EtOAc and the organic layer was dried over Na₂SO₄, filtered and concentrated under vacuum. The crude product (81 mg, 74% yield) was used for the next step without further purification. ¹H NMR (400 MHz, CDCl₃) δ 8.97 (d, ³J = 4.6 Hz, 1H), 8.65 (d, ³J = 5.6 Hz, 1H), 7.61 (dd, ³J = 8.6 Hz, ³J = 5.4 Hz, 2H), 7.56 (d, ³J = 4.6 Hz, 1H), 7.35 (d, ³J = 5.6

Hz, 1H), 7.24 (mt, 2H), 6.02 (s, 2H), 3.42 (s, 3H); MS (ESI) m/z (%): 385.1 (100) [M+H]⁺; UPLC purity = 79%, Rt 1.92 min.

4.1.9. 3-(2-Aminopyrimidin-4-yl)-2-(4-fluorophenyl)imidazo[1,2-a]pyrazin-8-amine (**24**)

In a vial were added compound **23** (70 mg, 0.18 mmol), ammonium hydroxide (3 mL, 25% in water) in 1,4-dioxane (3 mL). The vial was sealed and the suspension was heated at 110 °C for 1 h 15. After cooling, water was added the resulting mixture was extracted with EtOAc. The organic layer was dried over Na₂SO₄, filtered and concentrated under vacuum. Purification by flash chromatography (EtOAc) afforded **24** (25 mg, 43% yield) as a white powder. Mp: 128.5 °C; ¹H NMR (400 MHz, DMSO-*d*₆) δ 8.57 (d, ³*J* = 4.6 Hz, 1H), 8.16 (d, ³*J* = 5.4 Hz, 1H), 7.66 (mt, 2H), 7.35 (d, ³*J* = 4.6 Hz, 1H), 7.29 (mt, 2H), 7.07 (s, 2H), 6.92 (s, 2H), 6.34 (d, ³*J* = 5.4 Hz, 1H); ¹³C NMR (100 MHz, DMSO-*d*₆) δ 163.47, 162.15 (¹*J*_{C-F} = 245 Hz), 158.56, 156.75, 150.32, 144.10, 132.44, 131.06 (³*J*_{C-F} = 8 Hz, 2C), 130.58 (⁴*J*_{C-F} = 3 Hz), 129.29, 120.09, 115.45 (²*J*_{C-F} = 22 Hz, 2C), 110.35, 108.89; MS (TOF MS ES⁺) m/z (%): 322.12 (100) [M+H]⁺; UPLC purity = 100%, Rt 1.52 min; HRMS (TOF MS ES⁺): calcd. for C₁₆H₁₂FN₇ [M+H]⁺ 322.1216, found: 322.1208.

4.2. Molecular modelling

4.2.1 Homology modelling

The 2.0 Å resolution X-ray crystal structure of *Oryza sativa* CK1 with accession code 3SV0 was retrieved from the *Protein Data Bank*, and used as template for the construction of a homology model for the amino-acids sequence associated with entry Q9NHE1 from the UniProt database with the MODELLER v9.22 software package [28]. A range of structures of the *ab initio* C-terminal loop (not covered by the template) was generated using the same software, and the solution exhibiting the best score (and folding) was merged with the part obtained by homology to yield a complete model of the protein.

4.2.2 Molecular dynamics

The resulting homology model was placed within a simulation periodic box with a 1 nm margin. The protein was solvated with water molecules taken from a library of pre-equilibrated pure solvent model, and sodium chloride was added in sufficient quantity to reach electric neutrality as well as an ionic strength corresponding to a *c* = 150 mM salt concentration. Simulation was performed with GROMACS v2019.1 software package [29], using AMBER99SB-ILDN force field [30] in combination with the TIP3P water model [31].

The so-built system was energy-minimized using a steepest descent algorithm then subjected to two consecutive 100 ps MD simulations for equilibration purposes (the first one with Berendsen [32] and the second one with Nosé-Hoover [33] thermostat). Production MD simulation was then conducted with Nosé-Hoover thermostat and Parrinello-Rahman pressure coupling [34] for a total simulated time of 10 ns. Atom coordinates were saved every simulated 20 ps for trajectory analysis.

10 representative conformations of the binding site were selected after binding site residues RMSD-based clustering of the trajectory performed using the GROMOS algorithm [35] with a cut-off value of 0.66 Å.

4.2.3 Molecular docking

Initial coordinates for ligands were generated using the MarvinSketch v19.26 software package [36], and compounds were freely docked in a parallelepipedic box circumscribed to the ATP binding site using the AutoDock Vina v1.1.2 software package [37] in each of the 10 representative protein structures derived from the molecular dynamics calculation. Best-ranked solutions in terms of scoring function were retained for analysis and depiction using the UCSF Chimera v1.14 software package [38].

4.3. Biological evaluation

4.3.1 Antileishmanial activity

4.3.1.1 Cell lines and cultures

The mouse monocyte/macrophage cell line RAW264.7 was maintained in culture in DMEM supplemented with 10% heat-inactivated fetal bovine serum.

The *Leishmania* strains were obtained from CNRLeish (Centre National de Référence des *Leishmania*). Strains used for *in vitro* experiments were *Leishmania donovani* (MHOM/ET/67/HU3), *L. infantum* (MHOM/FR/2008/LEM5700), *L. major* (MHOM/PT/92/CRE26), *L. amazonensis* (MHOM/BR/73/M2269) and *L. braziliensis* (MHOM/BR/75/M2903b).

These strains were used for *in vitro* experiments. Promastigotes forms were grown in M-199 medium (Sigma-Aldrich) supplemented with 40 mM HEPES, 100 µM adenosine, 0.5 mg/mL haemin, 10% heat-inactivated foetal bovine serum (FBS) (Invitrogen Life Technologies) at 25°C in a dark environment under an atmosphere of 5% CO₂. For differentiation of promastigotes into axenic amastigotes, plateau-phase cultures of promastigotes were used and a suspension of parasites was prepared at 10⁷ parasites / mL in axenic amastigote medium (1 x M-199, supplemented with 40 mM HEPES, 100 µM adenosine, 0.5 mg/mL haemin, 10% FBS; 2 mM MgCl₂, 2 mM CaCl₂). The pH was adjusted to pH 5.5. Axenic amastigotes were grown at 37 °C in 5% CO₂. The axenic amastigote experiments were performed only after parasite differentiation.

Leishmania major (MHOM/IL/81/BNI) promastigotes were maintained by weekly subpassages in Schneider's insect medium (Sigma chemical Co. St Louis, Mo) supplemented with 13% heat-inactivated foetal bovine serum (FBS, Sigma–Aldrich) at 26 °C [39].

4.3.1.2 *In vitro* antileishmanial evaluation on intramacrophage amastigotes

The mouse monocyte/macrophage cell line RAW 264.7 was maintained in DMEM supplemented with 10% heat-inactivated fetal bovine serum. RAW 264.7 cells were seeded into a 96-well microtiter plate at a density of 100,000 cells/well in 100 µL of DMEM. After incubation in a 5% CO₂ incubator at 37 °C for 24 h, the culture medium was

replaced with 100 μ L of fresh DMEM containing a suspension of plateau-phase culture of promastigotes to reach a ratio parasite/macrophage of 16:1. In each plate, 8 wells contained axenic amastigotes (control of the parasite growth), 8 wells contained only macrophages (control of the macrophage growth) and finally 8 wells contained infected macrophages (control of the growth of intramacrophage parasites). After incubation in a 5 % CO₂ incubator at 37 °C for 24 h (the time needed by the parasite to infect the macrophage), cells were visualized using an inverted microscope to check the presence of inside parasites. Then, the culture medium was replaced with fresh DMEM to realize the serial dilution. Final concentrations of test compound were obtained by serial dilution ranging between 391 nM and 100 μ M for pure compounds. After incubation, cells were visualized using an inverted microscope to check the cell lysis, their morphology and the presence of outside parasites. The viability of the amastigotes into macrophages was then assessed using the SYBR1 Green I (Invitrogen, France) incorporation method. Thus, the medium was removed and the cells were lysed in 100 μ L lysis buffer. The plates were then subjected to 3 freeze-thaw cycles to achieve complete lysis. The parasite lysis suspension was diluted 1:1 in lysis buffer with SYBR Green I as previously described. The IC₅₀ value was calculated by nonlinear regression using icestimator website 1.2 version: <http://www.antimalarial-icestimator.net/MethodIntro.htm>. Fluorescence obtained was compared to those from the range obtained with parasite, infected cell and non-infected cell densities. The activity of the compounds was expressed as IC₅₀ (concentration of drug inhibiting the parasite growth by 50%, comparatively to the controls treated with the excipient only). Miltefosine was used as the reference drug.

For *Leishmania major* (MHOM/IL/81/BNI), compounds were diluted in dimethylsulfoxide (DMSO) in view to obtain stock solutions (10 mM). Dilutions of each compound were realized in medium in accordance with cell line culture and at a maximum final concentration of 1% DMSO. Activity against the intracellular amastigote stage of the parasite was determined after infection of Balb/c mice peritoneal macrophages (CE Janvier, Le Genest, France). 100 μ L of a peritoneal macrophage suspension were placed into a 24-well plate (Nunc®) on glass slides (10 mm diameter) at 1.5 $\times 10^5$ cell/mL in RPMI 1640 with 15% FBS at 37 °C and 5% CO₂. Following a 24 h-incubation to allow attachment, macrophages were infected with 100 μ L of a stationary phase promastigotes (1.5 $\times 10^6$ promastigotes/mL in RPMI 1640 medium plus 15% FBS) and then incubated for a 24 h-period at 37 °C and 5% CO₂ for infection. Macrophage culture was washed and exposed to drugs at concentrations of 100, 10, 1 and 0.1 μ M. After 4 days, cultures were fixed with methanol, stained with May-Grunwald-Giemsa and microscopically examined. The average number of amastigotes per macrophage was determined by counting the number of amastigotes in 100 randomly chosen macrophages in each duplicate well. IC₅₀ values were calculated by using the values of the number of amastigotes per macrophage [39]. Miltefosine was used as a reference at the concentrations of 100, 10 and 1 μ M. Experiments were done twice.

4.3.2 Cytotoxicity determination

4.3.2.1 Evaluation of compounds cytotoxicity using SYBR Green method

Cytotoxicity was evaluated on mouse monocyte/macrophage-like cell line RAW 264.7 (Cell collection CNRS UMR 8076 BioCis, University Paris-Saclay). The RAW 264.7 cells were cultured in Dulbecco's modified

Eagle's minimal essential medium (DMEM) (Invitrogen Life Technologies) supplemented with 10% heat-inactivated fetal bovine serum, at 37 °C in a humidified atmosphere containing 5% CO₂. Cells were seeded into a 96-well microtitration plate at a density of 100,000 cells/well in 100 µL. After incubation in a 5 % CO₂ incubator at 37 °C for 24 h, the culture medium was replaced with 100 µL of fresh DMEM containing two-fold serial dilutions of the tested compounds. Final concentrations of tested compounds or extracts were obtained by serial dilution ranging between 49 nM and 100 µM for pure compounds and between 49 ng/mL and 100 µg/mL for extracts. Miltefosine was used as the reference drug and cells without drug treatment as growth control. After incubation, cells were visualized using an inverted microscope to check their morphology and to control the drug solubility. After a 48 h incubation time at 37 °C with 5% CO₂, growth was determined by using SYBR Green 1 as previously described [40]. The cytotoxicity of the compounds was expressed as CC₅₀ (Cytotoxic Concentration 50%: concentration inhibiting the macrophages growth by 50%). The CC₅₀ was calculated by nonlinear regression using icestimator website 1.2 version: <http://www.antimalarial-icestimator.net/MethodIntro.htm>.

4.3.2.2. Cytotoxicity assay on MRC-5 fibroblast cells

Cytotoxicity of compounds was studied with human fibroblast (MRC-5). Cells were grown in RPMI 1640 medium (Sigma-aldrich) supplemented with 10% foetal bovin serum (Sigma-aldrich). Drugs were tested at three concentrations (100, 10 and 1 µM) in triplicate for a 96 h-incubation time. Cytotoxicity was measured on the Fluorolite 1000 (Dynatech, France) after a 4-h incubation time with 10 µL of resazurin solution (700 µM). Inhibitory concentration 50 (IC₅₀) is a mean of triplicate values [41,42].

4.3.2.3. Evaluation of compounds cytotoxicity using in vivo Galleria mellonella model

G. mellonella larvae were bred in IICiMed laboratory at 30-32 °C in a mixture of flour, honey, oat meal, glycerol and pollen until 260 to 320 mg (6th developmental stage). Groups of ten larvae were randomly selected for the experiments. Each larva was injected in the 4th left pro-leg with 10 µL of antifungal compounds or an equivalent volume of PBS/DMSO for control group at a dose varying between 10 mg/kg and 50 mg/kg using a 0.3 mL - 30G-Insulin syringe. Larvae were incubated in the dark at 37 °C and survival was evaluated daily for 7 days. Death was assessed by the lack of movement in response to stimulus, with or without discolouration. Percentage survival was plotted using GraphPad Prism and survival analyses were determined using the log-rank test and the Kaplan-Meier survival curves. Two independent experiments were performed.

4.3.3 Kinase inhibition assays

Two different methods were used to study the effect of the compounds on kinase activities: (i) a radiometric assay using [γ -³³P] ATP and (ii) a luminescent ADP detection assay (ADP-Glo assay, Promega, Madison, WI).

4.3.3.1. Experimental details on the radiometric assay

Kinase activities were assayed in appropriate kinase buffer, with either protein or peptide as substrate in the presence of 15 μM [γ - ^{33}P] ATP (3,000 Ci/mmol; 10 mCi/mL) in a final volume of 30 μL following the assay described in [43]. Controls were performed with appropriate dilutions of dimethylsulfoxide (DMSO). Full-length kinases are used unless specified. Peptide substrates were obtained from ProteoGenix (Schiltigheim, France) or Sigma for Histone H1 (#H5505), Casein (#C4032) and MBP (#M1891).

4.3.3.2 Experimental details on ADP-Glo™ assay

Kinase enzymatic activities were assayed in 384-well plates using the ADP-Glo™ assay kit (Promega, Madison, WI) according to manufacturer's recommendations ([44] for details on this method). Briefly, reactions were carried out in a final volume of 6 μL for 30 min at 30 °C in appropriate kinase buffer, with either protein or peptide as substrate in the presence of 10 μM ATP. The experimental conditions used to perform the various kinase assays are reported in [45]. In order to determine the half maximal inhibitory concentration (IC_{50}), the assays were performed in duplicate in the absence or presence of increasing doses of the tested compounds. Kinase activities are expressed in % of maximal activity, i.e. measured in the absence of inhibitor. IC_{50} values were determined from the dose response curves using Prism-GraphPad (GraphPad Software, San Diego, CA, USA).

Buffers: (A) 10 mM MgCl_2 , 1 mM EGTA, 1 mM DTT, 25 mM Tris-HCl pH 7.5, 50 $\mu\text{g}/\text{mL}$ heparin; (B) 5 mM MOPS pH 7.2, 2.5 mM β -glycerophosphate, 4 mM MgCl_2 , 2.5 mM MnCl_2 , 1 mM EGTA, 0.5 mM EDTA, 50 $\mu\text{g}/\text{mL}$ BSA, 0.05 mM DTT; (C) 25 mM MOPS, pH7.2, 12.5 mM β -glycerophosphate, 25 mM MgCl_2 , 5 mM EGTA, 2 mM EDTA, 0.25 mM DTT.

Native or recombinant protein kinases used during this study were:

LmCK1 (LmjF35.1010, from *Leishmania major*, recombinant, expressed in bacteria [12], was assayed in buffer A with 170 μM of the following peptide: RRKHAAGSpAYSITA ("Sp" stands for phosphorylated serine) as CK1-specific substrate.

HsCK1 ϵ (human, recombinant, expressed by baculovirus in Sf9 insect cells) was assayed in buffer A with 170 μM of the following peptide: RRKHAAGSpAYSITA.

HsCDK2/CyclinA (human, cyclin-dependent kinase-2, kindly provided by Dr. A. Echaliier-Glazer, Leicester, UK) was assayed in buffer A with 37.2 μM of histone H1 as substrate.

HsCDK5/p25 (human, recombinant, expressed in bacteria) was assayed in buffer A, with 37.2 μM of histone H1 as substrate.

HsCDK9/CyclinT (human, recombinant, expressed by baculovirus in Sf9 insect cells) was assayed in buffer A with 83 μM of the following peptide: YSPTSPSYSPSTSPSYSPSTSPSKKKK, as substrate.

SscGSK-3 α/β (*Sus scrofa domesticus*, native porcine enzyme, affinity purified from porcine brain) was assayed in buffer A with 20 μM of GS-1 peptide, a GSK-3-selective substrate (YRRAAVPPSPSLSRHSSPHQSpEDEEE).

HsPIM1 (human proto-oncogene, recombinant, expressed in bacteria) was assayed in buffer A with 18.6 μM of histone H1 (Sigma #H5505) as substrate.

HsRIPK3 (human, recombinant, expressed by baculovirus in Sf9 insect cells) was assayed in buffer B with 8.7 μM of MBP as substrate.

*Hs*HASPIN (human, kinase domain, amino acids 470 to 798, recombinant, expressed in bacteria) was assayed in buffer A with 8 μ M of Histone H3 (1-21) peptide (ARTKQTARKSTGGKAPRKQLA) as substrate.

*Hs*AURKB (human Aurora kinase B, recombinant, expressed by baculovirus in Sf9 insect cells, SignalChem, product #A31-10G) was assayed in buffer C with 8.7 μ M of MBP as substrate.

*Mm*CLK1 (from *Mus musculus*, recombinant, expressed in bacteria) was assayed in buffer A with 57.3 μ M of the following peptide: GRSRSRSRSRSR as substrate.

*Rn*DYRK1A (*Rattus norvegicus*, amino acids 1 to 499 including the kinase domain, recombinant, expressed in bacteria, DNA vector kindly provided by Dr. W. Becker, Aachen, Germany) was assayed in buffer A with 10.7 μ M of the following peptide : KKISGRLSPIMTEQ as substrate.

Controls inhibitors:

To validate each kinase assay, the following model inhibitors were used under the same conditions than the tested compounds: Barasertib (AZD1152-HQPA, #S1147, Selleckchem) for AuroraB; Staurosporine from *Streptomyces* sp. (#S5921, purity 95%, Sigma-Aldrich) for CK1 ϵ and *Lm*CK1; Indirubin-3'-oxime (#I0404, Sigma-Aldrich) for CDK2/CyclinA, CDK5/p25, CDK9/CyclinT, *Ssc*GSK-3 α/β , *Rn*DYRK1A and *Mm*CLK1; CHR-6494 (#SML0648, Sigma-Aldrich) for HASPIN; GSK'872 (GSK2399872A, #S8465, Selleckchem) for RIPK3; SGI-1776 (#S2198, Selleckchem) for PIM1.

Acknowledgements

The authors gratefully acknowledge the Consortium against Parasites and Fungi (CaPF) for the scientific exchanges.

Authors acknowledge the Corsaire-ThalassOMICS Metabolomics Facility (Biogenouest, University of Nantes, France) and UMR 6230 CEISAM Laboratory for HRMS analyses.

The authors also thank GIS IBiSA (Infrastructures en Biologie Santé et Agronomie, France) and Biogenouest (Western France life science and environment core facility network) for supporting kinase screening facility (KISSf, Roscoff, France).

Supplementary data

Supplementary data related to this article can be found at...

References

- [1] World Health Organization, Leishmaniasis, updated July 2020. Information site: <https://www.who.int/en/news-room/fact-sheets/detail/leishmaniasis>.
- [2] S. Burza, S.L. Croft, M. Boelaert, Leishmaniasis, *Lancet* 392 (2018) 951–70. Doi: 10.1016/S0140-6736(18)31204-2
- [3] B.M. Roatt, J.M. de Oliveira Cardoso, R.C.F. De Brito, W. Coura-Vital, R.D. de Oliveira Aguiar-Soares, A. Barbosa Reis, Recent advances and new strategies on leishmaniasis treatment. *Appl. Microbiol. Biotechnol.* 104 (2020) 8965–8977. Doi: 10.1007/s00253-020-10856-w

- [4] E. Lindgren, Y. Andersson, J.E. Suk, B. Sudre, J.C. Semenza, Monitoring EU emerging infectious disease risk due to climate change, *Science* 336 (2012) 418–419. Doi: 10.1126/science.1215735
- [5] M. Akhoundi, K. Kuhls, A. Cannet, J. Votýpka, P. Marty, P. Delaunay, D. Sereno, A historical overview of the classification, evolution, and dispersion of *Leishmania* parasites and sandflies, *PLoS Negl. Trop. Dis.* 10 (2016) e0004349. Doi:10.1371/journal.pntd.0004349
- [6] R. Birnbaum, N. Craft, Innate immunity and *Leishmania* vaccination strategies, *Dermatol. Clin.* 29 (2011) 89–102. Doi: 10.1016/j.det.2010.08.014
- [7] D. M. Claborn, The biology and control of leishmaniasis vectors, *J. Glob. Infect. Dis.* 2 (2010) 127–134. Doi: 10.4103/0974-777X.62866
- [8] R.M. Reguera, Y. Pérez-Pertejo, C. Gutiérrez-Corbo, B. Domínguez-Asenjo, C. Ordóñez, C. García-Estrada, M. Martínez-Valladares, R. Balaña-Fouce, Current and promising novel drug candidates against visceral leishmaniasis, *Pure Appl. Chem.* 91 (2019) 1385–1404. Doi: 10.1515/pac-2018-1102
- [9] R. Balaña-Fouce, M.Y. Pérez Pertejo, B. Domínguez-Asenjo, C. Gutiérrez-Corbo, R.M. Reguera, Walking a tightrope: drug discovery in visceral leishmaniasis, *Drug Discov. Today* 24 (2019) 1209–1216. Doi: 10.1016/j.drudis.2019.03.007
- [10] S. Marhadour, P. Marchand, F. Pagniez, M.-A. Bazin, C. Picot, O. Lozach, S. Ruchaud, M. Antoine, L. Meijer, N. Rachidi, P. Le Pape, Synthesis and biological evaluation of 2,3-diarylimidazo[1,2-*a*]pyridines as antileishmanial agents, *Eur. J. Med. Chem.* 58 (2012) 543–556. Doi: 10.1016/j.ejmech.2012.10.048
- [11] P. Marchand, M.-A. Bazin, F. Pagniez, G. Rivière, L. Boderio, S. Marhadour, M.-R. Nourrisson, C. Picot, S. Ruchaud, S. Bach, B. Baratte, M. Sauvain, D. Castillo Pareja, A.J. Vaisberg, P. Le Pape, Synthesis, antileishmanial activity and cytotoxicity of 2,3-diaryl- and 2,3,8-trisubstituted imidazo[1,2-*a*]pyrazines, *Eur. J. Med. Chem.* 103 (2015) 381–395. Doi: 10.1016/j.ejmech.2015.09.002
- [12] N. Rachidi, J.-F. Taly, E. Durieu, O. Leclercq, N. Aulner, E. Prina, P. Pescher, C. Notredame, L. Meijer, G.F. Späth, Pharmacological assessment defines *Leishmania donovani* casein kinase 1 as a drug target and reveals important functions in parasite viability and intracellular infection, *Antimicrob. Agents Chemother.* 58 (2014) 1501–1515. Doi: 10.1128/AAC.02022
- [13] E. Durieu, E. Prina, O. Leclercq, N. Oumata, N. Gaboriaud-Kolar, K. Vougiannopoulou, N. Aulner, A. Defontaine, J.H. No, S. Ruchaud, A.L. Skaltsounis, H. Galons, G.F. Späth, L. Meijer, N. Rachidi, From drug screening to target deconvolution: a target-based drug discovery pipeline using *Leishmania* casein kinase 1 isoform 2 to identify compounds with antileishmanial activity, *Antimicrob. Agents Chemother.* 60 (2016) 2822–2833. Doi: 10.1128/AAC.00021-16
- [14] J.M. Silverman, J. Clos, C. Camargo de Oliveira, O. Shirvani, Y. Fang, C. Wang, L.J. Foster, N.E. Reiner, An exosome-based secretion pathway is responsible for protein export from *Leishmania* and communication with macrophages, *J. Cell Sci.* 123 (2010) 123, 842–852. Doi: 10.1242/jcs.056465
- [15] J. Liu, L.P. Carvalho, S. Bhattacharya, C.J. Carbone, K.G. Suresh Kumar, N.A. Leu, P. M. Yau, R.G.K. Donald, M.J. Weiss, D.P. Baker, K.J. McLaughlin, P. Scott, S.Y. Fuchs, Mammalian casein kinase 1 α and its leishmanial ortholog regulate stability of IFNAR1 and type I interferon signaling, *Mol. Cell Biol.* 29 (2009) 6401–6412. Doi: 10.1128/MCB.00478-09

- [16] T. Böhm, Z. Meng, P. Haas, D. Henne-Bruns, N. Rachidi, U. Knippschild, J. Bischof, The kinase domain of CK1 δ can be phosphorylated by Chk1, *Biosci. Biotechnol. Biochem.* 83 (2019) 1663–1675. Doi: 10.1080/09168451.2019.1617105
- [17] A. Ceballos Garzon, D. Amado, E. Robert, C.M. Parra Giraldo, P. Le Pape, Impact of calmodulin inhibition by fluphenazine on susceptibility, biofilm formation and pathogenicity of caspofungin-resistant *Candida glabrata*, *J. Antimicrob. Chemother.* 75 (2020) 1187–1193. Doi: 10.1093/jac/dkz565
- [18] J.J. Allocco, R. Donald, T. Zhong, A. Lee, Y.S. Tang, R.C. Hendrickson, P. Liberator, B. Nare, Inhibitors of casein kinase 1 block the growth of *Leishmania major* promastigotes *in vitro*, *Int. J. Parasitol.* 36 (2006) 1249–1259. Doi: 10.1016/j.ijpara.2006.06.013
- [19] A.J. Majeed, O. Antonsen, T. Benneche, K. Undheim, Stannylation reactions and cross-couplings in pyrimidines, *Tetrahedron* 45 (1989) 993–1006. Doi: 10.1016/0040-4020(89)80011-0
- [20] B. Liégeault, D. Lapointe, L. Caron, A. Vlassova, K. Fagnou, Establishment of broadly applicable reaction conditions for the palladium-catalyzed direct arylation of heteroatom-containing aromatic compounds, *J. Org. Chem.* 74 (2009) 1826–1834. Doi: 10.1021/jo8026565
- [21] S. Marhadour, M.-A. Bazin, P. Marchand, An efficient access to 2,3-diarylimidazo[1,2-*a*]pyridines via imidazo[1,2-*a*]pyridine-2-yltriflate through a Suzuki cross-coupling reaction-direct arylation sequence, *Tetrahedron Lett.* 53 (2012) 297–300. Doi: 10.1016/j.tetlet.2011.11.015
- [22] A. Scribner, R. Dennis, S. Lee, G. Ouvry, D. Perrey, M. Fisher, M. Wyratt, P. Leavitt, P. Liberator, A. Gurnett, C. Brown, J. Mathew, D. Thompson, D. Schmatz, T. Biftu, Synthesis and biological activity of imidazopyridine anticoccidial agents: Part II, *Eur. J. Med. Chem.* 43 (2008) 1123–1151. Doi: 10.1016/j.ejmech.2007.09.013
- [23] L.M. Alcântara, T.C.S. Ferreira, V. Fontana, E. Chatelain, C.B. Moraes, L.H. Freitas-Junior, A multi-species phenotypic screening assay for leishmaniasis drug discovery shows that active compounds display a high degree of species-specificity, *Molecules* 25 (2020) 2551. Doi:10.3390/molecules25112551
- [24] R. Don, J.-R. Ioset, Screening strategies to identify new chemical diversity for drug development to treat kinetoplastid infections, *Parasitology* 141 (2014) 140–146. Doi: 10.1017/S003118201300142X.
- [25] E. Allegra, R.W. Titball, J. Carter, O.L. Champion, *Galleria mellonella* larvae allow the discrimination of toxic and non-toxic chemicals, *Chemosphere* 198 (2018) 469–472. Doi: 10.1016/j.chemosphere.2018.01.175
- [26] K. Kavanagh, E.P. Reeves, Exploiting the potential of insects for *in vivo* pathogenicity testing of microbial pathogens, *FEMS Microbiol. Rev.* 28 (2004) 101–12. Doi: 10.1016/j.femsre.2003.09.002
- [27] cLog P were predicted using VG method of MarvinSketch v. 15.3.16 (ChemAxon Ltd., Cambridge, MA, USA).
- [28] A. Šali, T.L. Blundell, Comparative protein modelling by satisfaction of spatial restraints, *J. Mol. Biol.* 234 (1993), 779–815. Doi:10.1006/jmbi.1993.1626
- [29] M.J. Abraham, T. Murtola, R. Schulz, S. Páll, J.C. Smith, B. Hess, E. Lindahl, GROMACS: High performance molecular simulations through multi-level parallelism from laptops to supercomputers, *SoftwareX* 1–2 (2015) 19–25. Doi:10.1016/j.softx.2015.06.001
- [30] K. Lindorff-Larsen, S. Piana, K. Palmo, P. Maragakis, J.L. Klepeis, R.O. Dror, D.E. Shaw, Improved side-chain torsion potentials for the Amber ff99SB protein force field, *Proteins* 78 (2010) 1950–1958. Doi:10.1002/prot.22711

- [31] W.L. Jorgensen, J. Chandrasekhar, J.D. Madura, R.W. Impey, M.L. Klein, Comparison of simple potential functions for simulating liquid water, *J. Chem. Phys.* 79 (1983) 926–935. Doi:10.1063/1.445869
- [32] H.J.C. Berendsen, J.P.M. Postma, W.F. van Gunsteren, A. DiNola, J.R. Haak, Molecular dynamics with coupling to an external bath, *J. Chem. Phys.* 81 (1984) 3684–3690. Doi:10.1063/1.448118
- [33] S. Nosé, M.L. Klein, Constant pressure molecular dynamics for molecular systems, *Mol. Phys.* 50 (1983) 1055–1076. Doi:10.1080/00268978300102851
- [34] M. Parrinello, A. Rahman, Polymorphic transitions in single crystals: A new molecular dynamics method, *J. Appl. Phys.* 52 (1981) 7182–7190. Doi:10.1063/1.328693
- [35] X. Daura, K. Gademann, B. Jaun, D. Seebach, W.F. van Gunsteren, A.E. Mark, Peptide folding: when simulation meets experiment, *Angew. Chem. Int. Ed.* 38 (1999) 236–240. Doi:10.1002/(SICI)1521-3773(19990115)38:1/2%3C236::AID-ANIE236%3E3.0.CO;2-M
- [36] MarvinSketch is developed by ChemAxon <<https://www.chemaxon.com>>.
- [37] O. Trott, A.J. Olson, AutoDock Vina: Improving the speed and accuracy of docking with a new scoring function, efficient optimization, and multithreading, *J. Comput. Chem.* 31 (2010) 455–461. Doi:10.1002/jcc.21334
- [38] UCSF Chimera is developed by the Resource for biocomputing, visualization, and informatics at the University of California, San Francisco, with support from NIH P41-GM103311. E.F. Pettersen, T.D. Goddard, C.C. Huang, G.S. Couch, D.M. Greenblatt, E.C. Meng, T.E. Ferrin, UCSF Chimera—A visualization system for exploratory research and analysis, *J. Comput. Chem.* 25 (2004), 1605–1612. Doi:10.1002/jcc.20084
- [39] F. Pagniez, H. Abdala-Valencia, P. Marchand, M. Le Borgne, G. Le Baut, S. Robert-Piessard, P. Le Pape, Antileishmanial activities and mechanisms of action of indole-based azoles, *J. Enzym. Inhib. Med. Chem.* 21 (2006) 277–283. Doi: 10.1080/14756360600700517
- [40] K. Seifert, S.L. Croft, *In vitro* and *in vivo* interactions between miltefosine and other antileishmanial drugs, *Antimicrob. Agents Chemother.* 50 (2006) 73–79. Doi: 10.1128 / AAC. 50.1.73-79.2006
- [41] F. Pagniez, N. Lebouvier, Y.M. Na, I. Ourliac-Garnier, C. Picot, M. Le Borgne, P. Le Pape, Biological exploration of a novel 1,2,4-triazole-indole hybrid molecule as antifungal agent, *J. Enzym. Inhib. Med. Chem.* 35 (2020) 398–403. Doi: 10.1080/14756366.2019.1705292
- [42] M. Van den Kerkhof, D. Mabile, E. Chatelain, C.E. Mowbray, S. Braillard, S. Hendrickx, L. Maes, G. Caljon, *In vitro* and *in vivo* pharmacodynamics of three novel antileishmanial lead series, *Int. J. Parasitol. Drugs Drug Resist.* 8 (2018) 81–86. Doi: 10.1016/j.ijpddr.2018.01.006
- [43] S. Bach, M. Knockaert, J. Reinhardt, O. Lozach, S. Schmitt, B. Baratte, M. Koken, S.P. Coburn, L. Tang, T. Jiang, D.C. Liang, H. Galons, J.F. Dierick, L.A. Pina, F. Meggio, F. Totzke, C. Schächtele, A.S. Lerman, A. Carnero, Y. Wan, N. Gray, L. Meijer, Roscovitine targets, protein kinases and pyridoxal kinase, *J. Biol. Chem.* 280 (2005) 31208–31219. Doi: 10.1074/jbc.M500806200
- [44] H. Zegzouti, M. Zdanovskaia, K. Hsiao, S.A. Goueli, ADP-Glo: A Bioluminescent and homogeneous ADP monitoring assay for kinases. *Assay Drug. Dev. Technol.* 7 (2009) 560-572. Doi: 10.1089/adt.2009.0222
- [45] N. Ibrahim, P. Bonnet, J.-D. Brion, J.-F. Peyrat, J. Bignon, H. Levaique, B. Josselin, T. Robert, P. Colas, S. Bach, S. Messaoudi, M. Alami, A. Hamze, Identification of a new series of Flavopiridol-like structures as kinase inhibitors with high cytotoxic potency, *Eur. J. Med. Chem.* 199 (2020) 112355. Doi: 10.1016/j.ejmech.2020.112355

Captions

Figure 1. Chemical structures of some antileishmanial compounds entering Phase I clinical trials

Figure 2. Modulation from the hit compound **CTN1122**

Scheme 1. Synthesis of compounds **2-11**.

Reagents and conditions: (a) NH₄OH, sealed tube, 100 °C, 17 h, 70%; (b) BrCH₂CO(4-RC₆H₄), CH₃CN, 80 °C, 11 h, 58% (**3**) and 18 h, 55% (**4**); (c) NIS, DMF, 60 °C, N₂, 7 h, 84%; (d) Dimethylamine 40% aq., K₂CO₃, DMF, sealed tube, 100 °C, 5 h, 70%; (e) (Het)ArB(OH)₂, PdCl₂(dppf), K₃PO₄, dioxane/H₂O (9:1), sealed tube, 100 °C, 20 h, 24–85%.

Table 1 Yields of Suzuki coupling reaction to obtain imidazo[1,2-*a*]pyrazines **7-11** from compound **6**.

Scheme 2. Synthesis of compounds **13-21**.

Reagents and conditions: (a) 1) HI (57% aq), rt, 72 h; 2) H₂O, NaHCO₃, 95%; (b) **13**, Pd(OAc)₂, PPh₃, Cs₂CO₃, DMF, 90 °C, 20 h, 31% (**14**) and 15 h, 47% (**15**); (c) Dimethylamine 40% aq., K₂CO₃, DMF, sealed tube, 90 °C, 4–17 h, 55–58%; (d) Oxone®, MeOH/H₂O, rt, 17–24 h, 25–98%; (e) NH₄OHaq, 1,4-dioxane, sealed tube, 110 °C, 9 h, 51% (**20**) and 1 h 30, 73% (**21**).

Scheme 3. Synthesis of compounds **22-24**.

Reagents and conditions: (a) NH₄OHaq, isopropanol, μ -wave, 120 °C, 1 h, 100%; (b) Oxone®aq, MeOH, rt, 24 h, 74 %; (c) NH₄OHaq, 1,4-dioxane, sealed tube, 110 °C, 1 h 15, 43%.

Table 2 *In vitro* antileishmanial activities against intracellular *L. major*, *L. amazonensis* and *L. braziliensis* amastigotes and cytotoxicity evaluation of imidazo[1,2-*a*]pyrazines **CTN1122**, **7-11**, **14-17**, **20-22** and **24**.

Table 3 *In vitro* antileishmanial activities against intracellular *L. infantum* and *L. donovani* amastigotes and cytotoxicity evaluation of imidazo[1,2-*a*]pyrazines **CTN1122**, **7-11**, **14-17**, **20-22** and **24**.

Figure 3. Evaluation of *in vivo* cytotoxicity of imidazo[1,2-*a*]pyrazines **CTN1122**, **7-11**, **14-17**, **20-22** and **24** on *G. mellonella* model. Percentage of survival 7 days after injection of a dose of 50 mg/kg for each compound. Mean of two independent experiments

Figure 4. Putative binding mode of **CTN1122** within the ATP binding site of a homology model of *Lm*CK1.

Table 4 Inhibition of *Leishmania major* CK1 and human CK1 activities of imidazo[1,2-*a*]pyrazines **CTN1122**, **7-11**, **14-17**, **20-22** and **24**, and their selectivity profile against an array of 10 native or recombinant protein kinases^a.

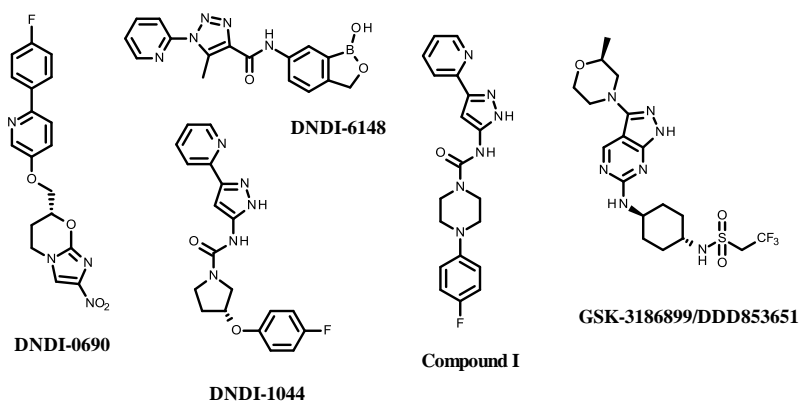


Figure 1. Chemical structures of some antileishmanial compounds entering Phase I clinical trials

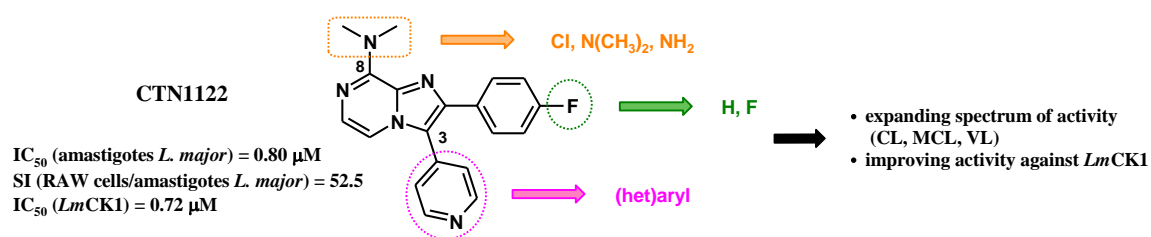
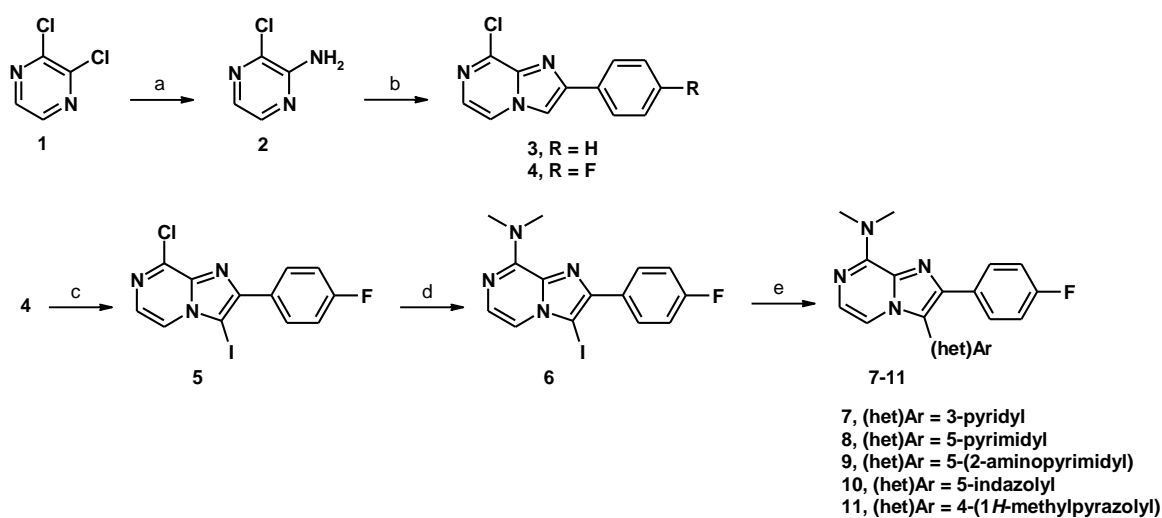


Figure 2. Modulation from the hit compound CTN1122

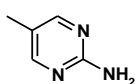
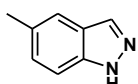
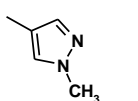


Scheme 1. Synthesis of compounds 2-11.

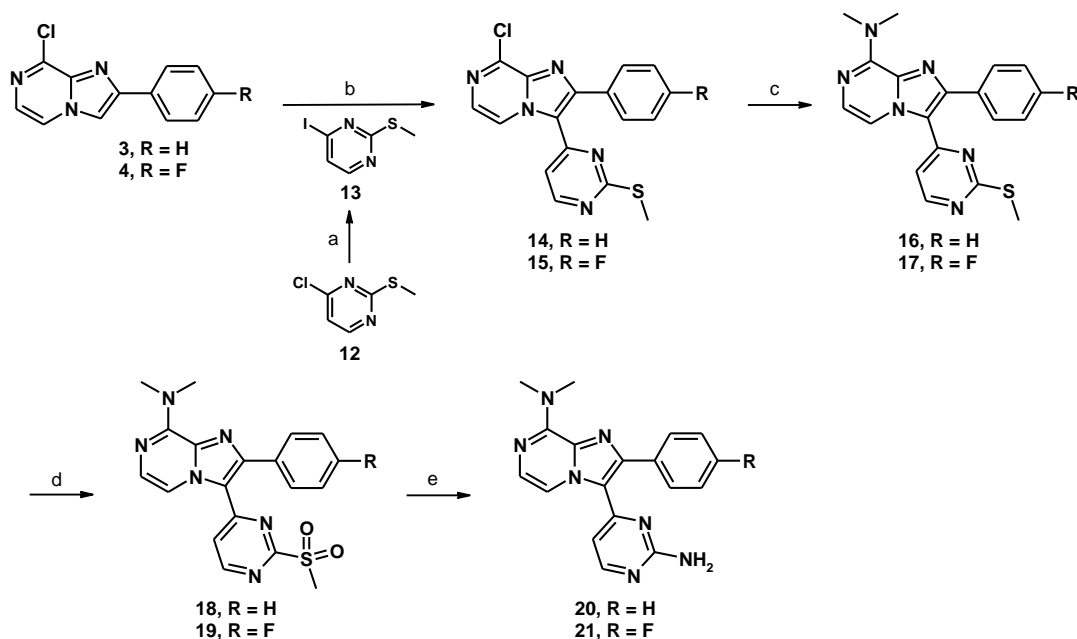
Reagents and conditions: (a) NH₄OH, sealed tube, 100 °C, 17 h, 70%; (b) BrCH₂CO(4-RC₆H₄), CH₃CN, 80 °C, 11 h, 58% (3) and 18 h, 55% (4); (c) NIS, DMF, 60 °C, N₂, 7 h, 84%; (d) Dimethylamine 40% aq., K₂CO₃, DMF, sealed tube, 100 °C, 5 h, 70%; (e) (Het)ArB(OH)₂, PdCl₂(dppf), K₃PO₄, dioxane/H₂O (9:1), sealed tube, 100 °C, 20 h, 24–85%.

Table 1 Yields of Suzuki coupling reaction to obtain imidazo[1,2-*a*]pyrazines 7-11 from compound 6.

Entry	(het)Ar	Compound	Yield (%) ^a
1		7	34
2		8	67

3		9	24
4		10	77
5		11	85

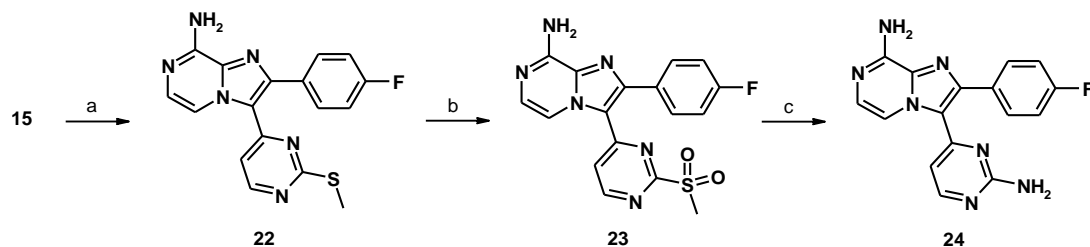
^a Isolated yields.



Scheme 2. Synthesis of compounds **13-21**.

Reagents and conditions: (a) 1) HI (57% aq), rt, 72 h; 2) H₂O, NaHCO₃, 95%; (b) **13**, Pd(OAc)₂, PPh₃, Cs₂CO₃, DMF, 90 °C, 20 h, 31% (**14**) and 15 h, 47% (**15**); (c) Dimethylamine 40% aq., K₂CO₃, DMF, sealed tube, 90 °C, 4–17 h, 55–58%; (d) Oxone®, MeOH/H₂O, rt, 17–24 h, 25–98%; (e) NH₄OHaq, 1,4-dioxane, sealed tube, 110 °C, 9 h, 51% (**20**) and 1 h 30, 73% (**21**).

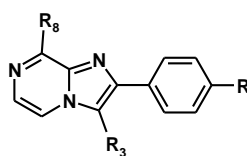
STANNYLATION REACTIONS AND CROSS-COUPPLINGS IN



Scheme 3. Synthesis of compounds **22-24**.

Reagents and conditions: (a) NH₄OHaq, isopropanol, μ -wave, 120 °C, 1 h, 100%; (b) Oxone®aq, MeOH, rt, 24 h, 74 %; (c) NH₄OHaq, 1,4-dioxane, sealed tube, 110 °C, 1 h 15, 43%.

Table 2 *In vitro* antileishmanial activities against intracellular *L. major*, *L. amazonensis* and *L. braziliensis* amastigotes and cytotoxicity evaluation of imidazo[1,2-*a*]pyrazines CTN1122, 7-11, 14-17, 20-22 and 24.



Cpd	R	R ₃	R ₈	Macrophages RAW 264.7 CC ₅₀ (μM) ^a ± SD	MRC-5 cells CC ₅₀ (μM) ^a	<i>L. major</i> IC ₅₀ (μM) ^a ± SD	SI ^b _{RAW}	SI ^c _{MRC-5}	<i>L. amazonensis</i> IC ₅₀ (μM) ^a ± SD	SI _{RAW}	SI _{MRC-5}	<i>L. braziliensis</i> IC ₅₀ (μM) ^a ± SD	SI _{RAW}	SI _{MRC-5}
		Miltefosine^d		43.01 ± 5.16	36.80 ± 5.20	1.44 ± 0.25	29.9	25.5	4.22 ± 0.25	10.2	8.7.	8.33 ± 2.00	5.2	4.4
CTN 1122	F		N(CH ₃) ₂	42.03 ± 4.5	>100	0.80 ± 0.20 ^d	52.5	>125	28.36 ± 4.64	1.5	3.5	57.92 ± 7.20	0.7	1.7
7	F		N(CH ₃) ₂	43.91 ± 3.94	48.85 ± 6.07	>50 ^e	n.d.	n.d.	>50	n.d.	n.d.	>50	n.d.	n.d.
8	F		N(CH ₃) ₂	39.12 ± 3.31	>100	33.58 ± 1.21 ^e	1.2	>3.0	>50	n.d.	n.d.	22.84 ± 3.06	1.7	4.4
9	F		N(CH ₃) ₂	48.95 ± 2.18	>100	>50 ^e	n.d.	n.d.	>50	n.d.	n.d.	>50	n.d.	n.d.
10	F		N(CH ₃) ₂	7.41 ± 2.36	24.79 ± 0.36	>12.5 ^e	0.6	2.0	>12.5	0.6	2.0	>12.5	0.6	2.0
11	F		N(CH ₃) ₂	15.95 ± 2.55	>100	8.99 ± 1.89 ^e	1.8	11.1	>25	0.6	4.0	>25	0.6	4.0
14	H		Cl	50.64 ± 1.30	33.5	>100 ^d	n.d.	n.d.	3.20 ± 1.25	15.8	10.5	17.65 ± 7.87	2.9	1.9
16	H		N(CH ₃) ₂	33.42 ± 2.88	81.0	>100 ^d	n.d.	n.d.	5.99 ± 1.35	5.6	13.5	45.58 ± 13.41	0.7	1.8
20	H		N(CH ₃) ₂	44.10 ± 2.98	58.4	28.32 ^d	1.5	2.1	23.35 ± 4.48	1.9	2.5	56.54 ± 15.7	0.8	1.0 n.d.
15	F		Cl	49.78 ± 2.79	79.9	>100 ^d	n.d.	n.d.	>100	n.d.	n.d.	74.02 ± 3.55	0.7	1.1
17	F		N(CH ₃) ₂	36.50 ± 1.22	67.0	>100 ^d	n.d.	n.d.	12.49 ± 1.65	2.9	5.4	63.52 ± 12.5	0.6	1.1
21	F		N(CH ₃) ₂	42.16 ± 1.08	100.0	8.24 ^d	5.1	12.1	6.12 ± 0.92	6.9	16.3	24.31 ± 2.75	1.7	4.1
22	F		NH ₂	11.51 ± 0.23	18.4	54.61 ^d	0.2	0.3	>12.5	>0.9	1.5	>12.5	>0.9	1.5
24	F		NH ₂	4.69 ± 0.99	32.8	34.12 ^d	0.1	1.0	*n.d.	n.d.	n.d.	*n.d.	n.d.	n.d.

^a Mean from two determinations.

^b SI_{RAW} = Cytotoxicity on RAW cells (CC₅₀)/Amastigotes (IC₅₀).

^c SI_{MRC-5} = Cytotoxicity on MRC-5 cells (CC₅₀)/Amastigotes (IC₅₀).

^d Miltefosine was used as antileishmanial reference drug. Its cytotoxicity on MRC-5 cells was in accordance with the literature [42].

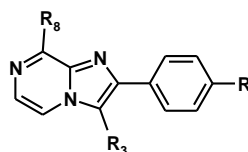
L. major strains MHOM/IL/81/BNT^d and MHOM/PT/92/CRE26^e.

n.d.: not determined.

SD: Standard Deviation.

*: toxicity on macrophages.

Table 3 *In vitro* antileishmanial activities against intracellular *L. infantum* and *L. donovani* amastigotes and cytotoxicity evaluation of imidazo[1,2-*a*]pyrazines **CTN1122**, **7-11**, **14-17**, **20-22** and **24**.



Cpd	R	R ₃	R ₈	Macrophages RAW 264.7 CC ₅₀ (μM) ^a ± SD	MRC-5 cells CC ₅₀ (μM) ^a	<i>L. infantum</i> IC ₅₀ (μM) ^a ± SD	SI ^b _{RAW}	SI ^c _{MRC-5}	<i>L. donovani</i> IC ₅₀ (μM) ^a ± SD	SI _{RAW}	SI _{MRC-5}
Miltefosine ^d				43.01 ± 5.16	36.80 ± 5.20	2.96 ± 0.31	14.5	12.4	1.83 ± 0.27	23.5	20.1
CTN 1122	F		N(CH ₃) ₂	42.03 ± 4.5	>100	12.80 ± 1.81	3.3	7.8	2.74 ± 0.14	15.3	36.5
7	F		N(CH ₃) ₂	43.91 ± 3.94	48.85 ± 6.07	>50	n.d.	n.d.	>50	n.d.	n.d.
8	F		N(CH ₃) ₂	39.12 ± 3.31	>100	>50	n.d.	n.d.	>50	n.d.	n.d.
9	F		N(CH ₃) ₂	48.95 ± 2.18	>100	>50	n.d.	n.d.	>50	n.d.	n.d.
10	F		N(CH ₃) ₂	7.41 ± 2.36	24.79 ± 0.36	12.92 ± 2.01	0.6	2.0	>12.5	0.6	2.0
11	F		N(CH ₃) ₂	15.95 ± 2.55	>100	2.60 ± 0.08	6.1	38.5	1.27 ± 0.03	12.6	78.7
14	H		Cl	50.64 ± 1.30	33.5	1.93 ± 0.11	26.2	17.3	9.82 ± 1.12	5.2	3.4
16	H		N(CH ₃) ₂	33.42 ± 2.88	81.0	12.54 ± 4.32	2.7	6.5	17.57 ± 1.52	1.9	4.6
20	H		N(CH ₃) ₂	44.10 ± 2.98	58.4	>100	n.d.	n.d.	>100	n.d.	n.d.
15	F		Cl	49.78 ± 2.79	79.9	>100	n.d.	n.d.	>100	n.d.	n.d.
17	F		N(CH ₃) ₂	36.50 ± 1.22	67.0	6.20 ± 0.84	5.9	10.8	10.39 ± 0.91	3.5	6.4
21	F		N(CH ₃) ₂	42.16 ± 1.08	100.0	6.55 ± 0.83	6.4	15.2	9.97 ± 5.39	4.2	10.0
22	F		NH ₂	11.51 ± 0.23	18.4	>12.5	>0.9	1.5	>12.5	>0.9	1.5
24	F		NH ₂	4.69 ± 0.99	32.8	*n.d.	n.d.	*n.d.	0.30 ± 0.03	15.6	109

^a Mean from two determinations.

^b SI_{RAW} = Cytotoxicity on RAW cells (CC₅₀)/Amastigotes (IC₅₀).

^c SI_{MRC-5} = Cytotoxicity on MRC-5 cells (CC₅₀)/Amastigotes (IC₅₀).

^d Miltefosine was used as antileishmanial reference drug. Its cytotoxicity on MRC-5 cells was in accordance with the literature [42].

n.d.: not determined.

SD: Standard Deviation.

*: toxicity on macrophages

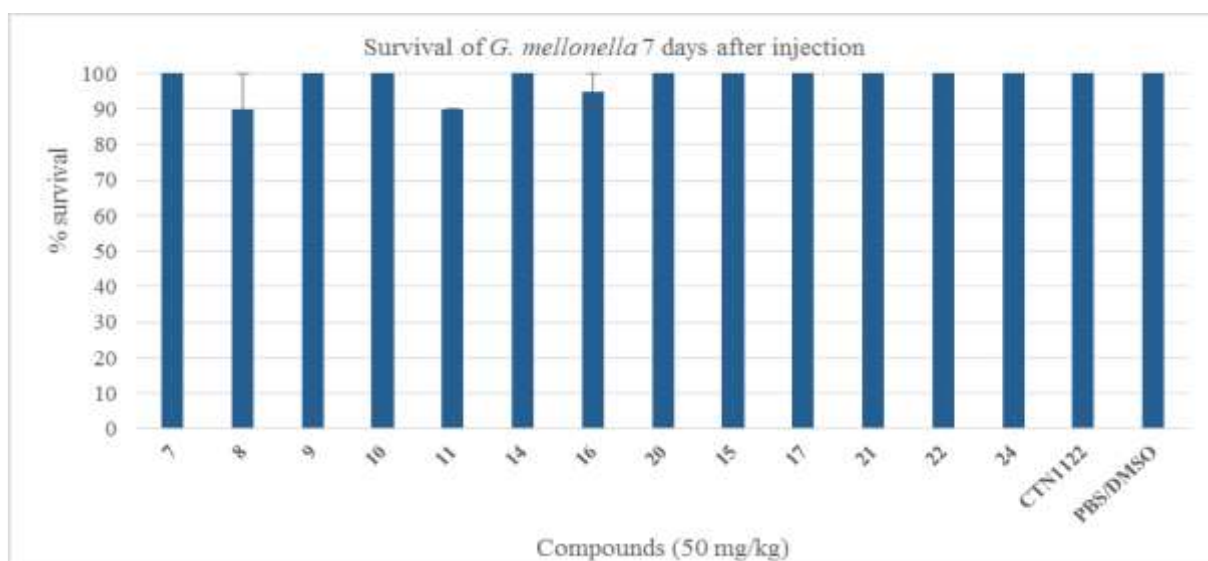


Figure 3. Evaluation of *in vivo* cytotoxicity of imidazo[1,2-*a*]pyrazines CTN1122, 7-11, 14-17, 20-22 and 24 on *G. mellonella* model. Percentage of survival 7 days after injection of a dose of 50 mg/kg for each compound. Mean of two independent experiments

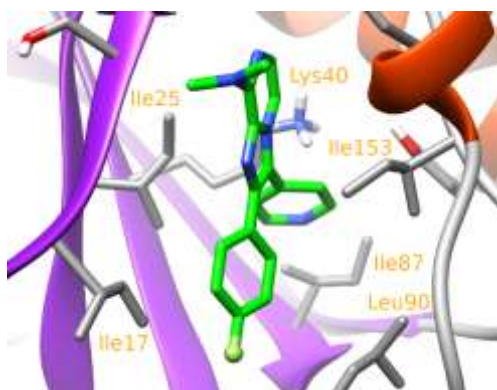
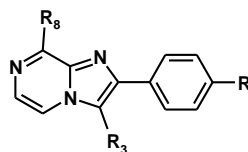


Figure 4. Putative binding mode of CTN1122 within the ATP binding site of a homology model of *LmCK1*.

Table 4 Inhibition of *Leishmania major* CK1 and human CK1 activities of imidazo[1,2-*a*]pyrazines **CTN1122**, **7-11**, **14-17**, **20-22** and **24**, and their selectivity profile against an array of 10 native or recombinant protein kinases^a.



Cpd	R	R ₃	R ₈	IC ₅₀ (μM) ^b <i>LmCK1</i>	IC ₅₀ (μM) ^b <i>HsCK1ε</i>	SI _{CK1} ^c	IC ₅₀ (μM) ^b <i>HsCDK2/</i> <i>CyclinA</i>	IC ₅₀ (μM) ^b <i>HsCDK5/</i> <i>p25</i>	IC ₅₀ (μM) ^b <i>HsCDK9/</i> <i>CyclinT</i>	IC ₅₀ (μM) ^b <i>SscGSK3α/β</i>	IC ₅₀ (μM) ^b <i>MmCLK1</i>
CTN1122	F		N(CH ₃) ₂	0.72	0.92	1.3	> 10	> 10	> 10	> 10	> 10
7	F		N(CH ₃) ₂	> 100	> 100	n.d.	> 10	> 10	> 10	> 10	> 10
8	F		N(CH ₃) ₂	29	> 100	n.d.	> 10	> 10	> 10	> 10	> 10
9	F		N(CH ₃) ₂	15.91	> 100	n.d.	> 10	> 10	> 10	> 10	> 10
10	F		N(CH ₃) ₂	1.88	2.08	1.1	> 10	> 10	> 10	> 10	> 10
11	F		N(CH ₃) ₂	12.42	> 100	n.d.	> 10	> 10	> 10	> 10	> 10
14	H		Cl	5.00	2.90	0.6	> 10	> 10	> 10	> 10	> 10
16	H		N(CH ₃) ₂	3.50	>10	> 2.8	> 10	> 10	> 10	> 10	0.90
20	H		N(CH ₃) ₂	0.035	1.05	30	> 10	> 10	> 10	> 10	0.59
15	F		Cl	> 10	> 10	n.d.	> 10	> 10	> 10	> 10	> 10
17	F		N(CH ₃) ₂	1.00	>10	> 10	> 10	> 10	> 10	> 10	> 10
21	F		N(CH ₃) ₂	0.042	0.16	3.8	> 10	> 10	> 10	> 10	0.25
22	F		NH ₂	0.65	0.18	0.3	10.0	1.00	> 10	4.50	0.16
24	F		NH ₂	0.04	0.20	5	0.80	10.0	0.50	1.10	0.035

^a All the compounds remained inactive against *HsPIM1*, *HsRIPK3*, *HsHASPIN* (except **11** IC₅₀ = 7.35 μM and **24** IC₅₀ = 4.5 μM), *HsAURKB*, *RnDYRK1A* (except **22** IC₅₀ = 2.0 μM). Kinase ADP-Glo™ assay for compounds **CTN1122**, **7-11** and kinase radiometric assay for compounds **14-24**, except for *HsCK1ε*

^b Mean from three determinations.

^c SI_{CK1} = IC₅₀ *HsCK1ε*/ IC₅₀ *LmCK1*.

Highlights

13 new imidazo[1,2-*a*]pyrazines related to CTN1122 were synthesized as antileishmanials

The most promising and safe compounds displayed low micromolar range potency against VL

L-CK1.2 homology model gave the first structural explanations of inhibitory activity

6 compounds showed low micromolar to nanomolar range L-CK1.2 inhibition

Graphical abstract

